In search for tuneable intramolecular intermetallic interactions in polynuclear lanthanide complexes†

Natalia Dalla Favera,[a] Laure Guénée,*[a] Gérald Bernardinelli[b] and Claude Piguet*[a]

Received 13th March 2009, Accepted 5th June 2009
First published as an Advance Article on the web 27th July 2009
DOI: 10.1039/b905131g

Reaction of unsymmetrical tridentate 2-benzimidazolyl-6-carboxamidopyridine binding units in the ligands **L4**[b] and **L5** with neutral $Ln(NO_3)_3$ (Ln is a trivalent lanthanide) gives mononuclear $[Ln(\mathbf{L4}^b)(NO_3)_3(solvent)]$ and binuclear $[Ln_2(\mathbf{L5})(NO_3)_6(solvent)_2]$ complexes. The crystal structures of **L4**[b] and $[Eu(\mathbf{L4}^b)(NO_3)_3(CH_3CN)]$ unravel the conformational change of the tridentate binding units required for its coordination to the metal, a process responsible for the change in electronic absorption spectra and in ^1H NMR spectra recorded in acetonitrile solution. In the solid state, the bis-tridentate ligand **L5** shows variable helical conformations of its central diphenylmethane spacer in its uncoordinated form (amphiverse helix) and in its complexed form in $[Eu_2(\mathbf{L5})(NO_3)_6(H_2O)_2]$ (regular helix), which puts the two metals at a contact distance of 8.564(1) Å. In solution, fast rearrangements yield an average planar extended conformation of the spacer, which increases the intramolecular intermetallic contact distance by 30% in $[Ln_2(\mathbf{L5})(NO_3)_6(H_2O)_2]$. Surprisingly, the thermodynamic analysis of the complexation processes in solution points to unusual, and to some extent non-predicted charge effects because the intramolecular intermetallic repulsive interaction measured in the neutral complex $[Ln_2(\mathbf{L5})(NO_3)_6]$ ($Ln\cdots Ln \approx 12$ Å) is comparable with that found in the highly charged triple-stranded helicate $[Ln_2(\mathbf{L5})_3]^{6+}$ ($Ln\cdots Ln \approx 9$ Å). The origin of this effect and its consequences on programming stable polynuclear complexes is discussed.

Introduction

The undeniable successes brought by supramolecular chemistry in the preparation of heterometallic *n*d–4f ($n = 3$–5) polynuclear complexes possessing predetermined structures, shapes and intermetallic communications[1] have not yet significantly influenced the parallel design of heterometallic 4f–4f′ analogues, because of the great similarity of the metallic coordination properties along the lanthanide series.[2] The rational preparation of pure heterometallic 4f–4f′ assemblies is thus currently limited to stepwise metallation/demetallation processes operating in kinetically inert lanthanide complexes including negatively charged ligands such as metallocryptands,[3] macrocyclic phthalocyanins and porphyrins[4] or highly pre-organized polycarboxylates.[5] Beyond the well-documented, but empirical investigations of deviations from statistical distributions resulting from the doping of different lanthanides into solid-state materials,[6] there is some rare, but remarkable and intriguing reports in the literature describing the characterization in solution and the isolation in the solid state of pure heterometallic 4f–4f′ polynuclear complexes obtained under apparent thermodynamic control (Fig. S1, ESI).†[7–11] The recurrent qualitative arguments for such fascinating selectivities rely on special size-discriminating or electrostatic effects resulting from the combination of two different types of binding units in the final polynuclear complexes. Whatever the origin of these minor variations, they are systematically assigned to some uncontrolled changes of the microscopic affinities $f_i^{Ln,L}$ (including desolvation) of the metal along the lanthanide series for each specific *i* binding site in the ligand (eqn (1) and eqn (2)).[12]

$$n\,\mathbf{L} + m\,Ln^{3+} \rightleftharpoons [Ln_m(\mathbf{L})_n^{3m+}] \quad \beta_{m,n}^{Ln,L} \tag{1}$$

$$\beta_{m,n}^{Ln,L} = e^{-\left(\Delta G_{m,n}^{Ln,L}/RT\right)} = \omega_{m,n}^{chiral}\cdot\omega_{m,n}^{Ln,L}\cdot\prod_{i=1}^{mn} f_i^{M,L}\cdot\prod_{i=1}^{mn-m-n+1} c_i^{eff}\cdot\prod_{i<j} e^{-\Delta E_{i,j}^{Ln,Ln}/RT}\cdot\prod_{k<l} e^{-\Delta E_{k,l}^{L,L}/RT} \tag{2}$$

A recent quantitative treatment of the competitive binding of different lanthanides in the triangular trinuclear complexes $[Ln^A_{(3-x)}Ln^B_x(\mathbf{L1}{-}3H)_2]^{3+}$ in water with eqn (2) indeed confirms that the microscopic affinity increases by two orders of magnitude in going from Ln = Nd ($\log(f_{N2O4}^{Nd,L1}) = 10.56$) to Ln = Eu ($\log(f_{N2O4}^{Eu,L1}) = 12.64$), while no significant variations in intermetallic interactions could be detected ($\Delta E_{1-2}^{Nd,Eu} = \Delta E_{1-2}^{Nd,Nd} = \Delta E_{1-2}^{Eu,Eu}$, Fig. 1).[13]

[a]*Department of Inorganic, Analytical and Applied Chemistry, University of Geneva, 30 quai E. Ansermet, CH-1211, Geneva 4, Switzerland. E-mail: claude.piguet@chiam.unige.ch*
[b]*Laboratory of X-Ray Crystallography, University of Geneva, 24 quai E. Ansermet, CH-1211, Geneva 4, Switzerland*

† Electronic supplementary information (ESI) available: Syntheses of the ligands **L4**[b] and **L5**, tables of selected bond lengths, bond angles and interplanar angles (Tables S1, S2, S4, S5, S10, S11), elemental analyses (Table S3), valence bond sums (Tables S6–S9), ^1H NMR chemical shifts (Table S12), fitted microscopic thermodynamic parameters (Table S13) and summary of crystallographic data (Table S14). Figures showing previous f–f′ assemblies obtained under thermodynamic control (Fig. S1), molecular structures and organizations of molecules in the crystallographic unit cells (Fig. S2–S5), ^1H NMR (Fig. S6) and spectrophotometric (Fig. S8) titration data, conformation of the spacer in solution (Fig. S7), symmetry numbers and statistical factors (Fig. S9) and emission spectra (Fig. S10–S12). CCDC reference numbers 723930–723933. For ESI and crystallographic data in CIF or other electronic format see DOI: 10.1039/b905131g

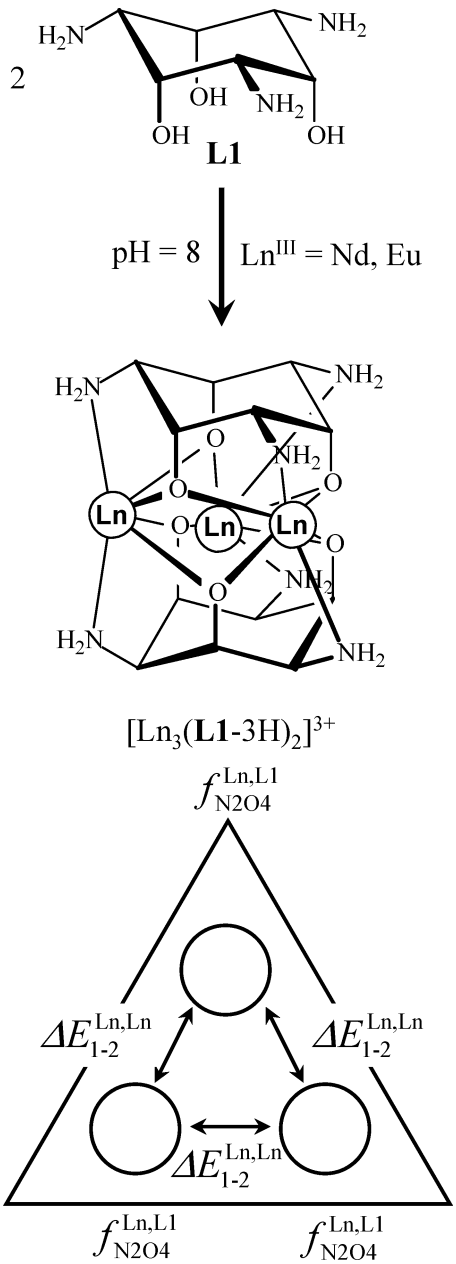

Fig. 1 Self-assembly of the trinuclear sandwich complexes $[Ln_3(\mathbf{L1}–3H)_2]^{3+}$ and its thermodynamic site-binding model ($f^{Ln,L1}_{N2O4}$ is the microscopic affinity of a lanthanide for the N_2O_4 binding site and $\Delta E^{Ln,Ln}_{1-2}$ represents the free energy of intermetallic interaction. Ln = Nd, Eu).[13]

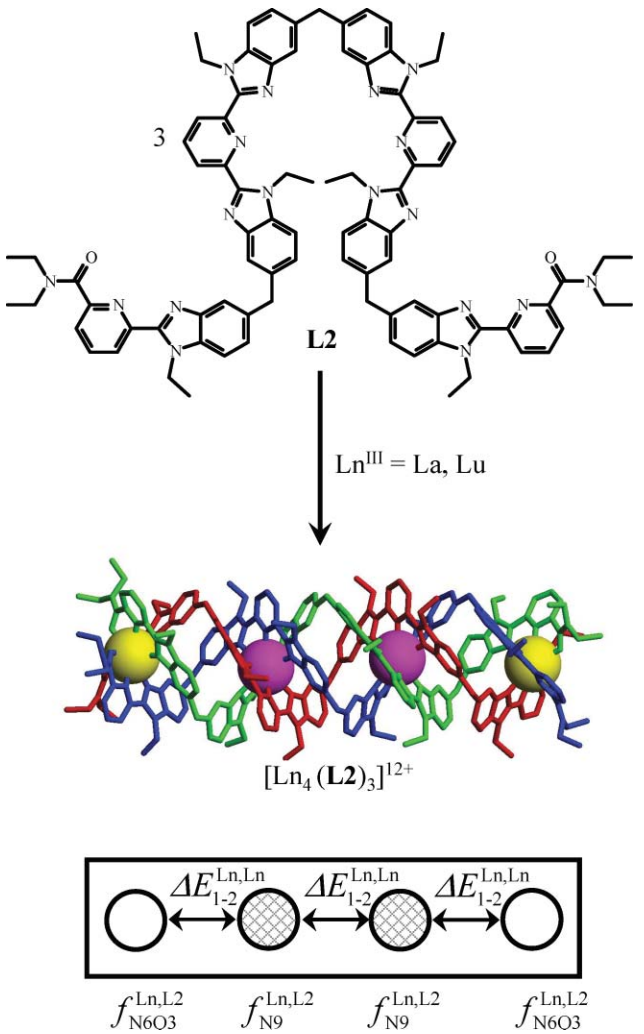

Fig. 2 Self-assembly of the tetranuclear triple-stranded helicates $[Ln_4(\mathbf{L2})]^{12+}$ and its thermodynamic site-binding model ($f^{Ln,L2}_{N6O3}$ and $f^{Ln,L2}_{N9}$ are the microscopic affinity of a lanthanide for the terminal N_6O_3, respectively the central N_9 binding sites. $\Delta E^{Ln,Ln}_{1-2}$ represents the free energy of geminal intermetallic interaction. Ln = La, Lu).[14]

However, a similar thermodynamic analysis of the distribution of the La/Lu pair in the tetranuclear helicates $[La_{(4-x)}Lu_x(\mathbf{L2})_3]^{12+}$ in acetonitrile with eqn (2) reaches the opposite conclusion, and the faint changes observed between the microscopic affinity of the central ($\log(f^{Ln,L2}_{N9})$) and that of the terminal ($\log(f^{Ln,L2}_{N6O3})$) sites for Ln = La and Lu cannot account for the distribution of the microspecies in solution (Fig. 2).[14] An additional driving force favours the close location of different lanthanides along the helical axis, which is unambiguously assigned to the smaller geminal intramolecular intermetallic repulsion operating between different metals: $\Delta E^{La,Lu}_{1-2} < \left(\Delta E^{La,La}_{1-2} + \Delta E^{Lu,Lu}_{1-2}\right)/2$.[14] Though this bias is of limited magnitude in these triple-stranded helicates (mixing rule: $\Delta E^{mix}_{1-2} = \left(\Delta E^{La,La}_{1-2} + \Delta E^{Lu,Lu}_{1-2}\right)/2 - \Delta E^{La,Lu}_{1-2} = 2$ kJ mol^{-1}),[14] it reveals that both (i) the nature of the binding site (*via* $f_i^{Ln,L}$) and (ii) the intermetallic interactions (*via* $\Delta E^{Ln,Ln}$) can be exploited for programming lanthanide complexes under thermodynamic control.

The intimate mechanism controlling the absolute affinity $f_i^{Ln,L}$ is rather obvious, since it relies on the free energy balance between the bond breaking process required for the desolvation of both metal and binding sites, and the subsequent bond making process leading to the fixation of the metal in site *i*.[12,15] The physical origin of the intermetallic interaction $\Delta E^{Ln,Ln}$ is more subtle because this parameter reflects the balance between the unfavourable intramolecular electrostatic repulsion produced by the introduction of closely spaced cationic metals in the complex, and the favourable contribution to the global solvation energy brought by the increase of the total charge of the complex.[16] We have therefore launched into a research project, which aims at tuning these non-trivial thermodynamic descriptors by

using chemically-relevant molecular (*i.e.* electronic and structural) factors. As a first step toward this goal, we report here on the consequences of the replacement of the charged Ln^{3+} partners obtained from $Ln(CF_3SO_3)_3$ or $Ln(ClO_4)_3$ salts, with neutral $Ln(NO_3)_3$ metallic units for loading segmental ligands. We indeed reason that the use of the well-established neutral starting complexes $[Ln(NO_3)_3(CH_3CN)_{2-3}]$ in acetonitrile[17] should drastically affect both the intramolecular Coulomb electrostatic intermetallic repulsion and the global contribution to solvation energies in the final binuclear complexes, the two main factors that control $\Delta E^{Ln,Ln}$.[16] Previous studies have shown that the reaction of the tridentate 2,6-bis(benzimidazol-2-yl)pyridine binding unit (N_3) found in ligands **L3**$^{a-e}$ (Scheme 1) with $Ln(NO_3)_3$ indeed produces neutral mononuclear complexes $[Ln(\mathbf{L3})(NO_3)_3]$ in the solid state.[18] However, the solution behaviour of these complexes in organic solvent is more complicated with the observation of intricate mixtures containing $[Ln(\mathbf{L3})_n(NO_3)_{3-x}]^{x+}$ (n = 1–2, x = −1, 0, 1) and $[Ln_2(\mathbf{L3})_n(NO_3)_6]$ (n = 2–3),[18] in line with similar observations reported for the analogous lanthanide nitrato complexes with 2,2′:6′,2″-terpyridine.[19] Interestingly, we notice that the closely related, but unsymmetrical tridentate N_2O ligands **L4**$^{a-d}$ (Scheme 2) gave less stable complexes with Ln^{3+} (obtained from its perchlorate salt $Ln(ClO_4)_3$ in acetonitrile) than those obtained within the **L3** series,[20,21] a situation that could be turned to an advantage for limiting the number of species in solution upon reaction with $Ln(NO_3)_3$. In this contribution, we thus report on the detailed coordination and thermodynamic behaviour of the archetypal ligand **L4**^{b}, and of its bis-tridentate segmental derivative **L5** with $Ln(NO_3)_3$.

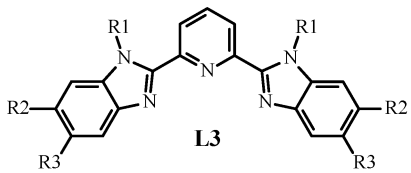

L3

R1	R2	R3	L
CH_3	H	H	**L3**^{a}
C_2H_5	H	H	**L3**^{b}
C_8H_{17}	H	H	**L3**^{c}
C_2H_5	O_2C-C_6H_5	H	**L3**^{d}
C_2H_5	H	O_2C-C_6H_5	**L3**^{e}

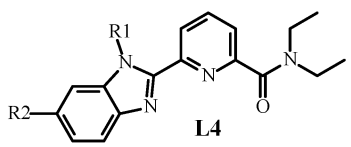

L4

R1	R2	L
CH_3	H	**L4**^{a}
C_2H_5	H	**L4**^{b}
3,5-$(CH_3O)C_6H_3CH_2$	H	**L4**^{c}
C_2H_5	CH_2OCH_3	**L4**^{d}

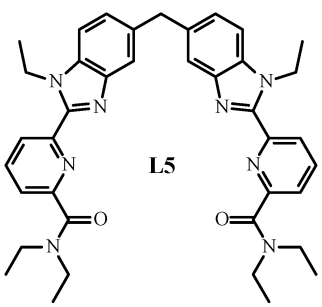

L5

Scheme 1 Chemical structures of ligands **L3**–**L5**.

Results and discussion

Preparation, characterization and solid-state structures of the ligands L4^{b} and L5, and of their complexes $[Ln(\mathbf{L4}^{b})(NO_3)_3]\cdot xH_2O$ and $[Ln_2(\mathbf{L5})(NO_3)_6]\cdot xH_2O$ (Ln = La, Eu, Gd, Tb, Lu, Y)

The ligands **L4**^{b} [20] and **L5**[22] are prepared following strategies previously developed for the introduction of unsymmetrical 2-benzimidazolyl-6-carboxamidopyridine units into extended segmental receptors (Scheme 2).[8,15,20,22]

Slow evaporation of an acetonitrile solution of **L4**^{b}, or diffusion of *n*-hexane into a concentrated dichloromethane solution of **L5** give colourless prisms whose X-ray crystal structures are shown in Fig. 3. Bond lengths and bond angles are standard (Tables S1 and S2, ESI),†[23] and the tridentate binding units systematically adopt the expected *trans–trans* conformation, which minimize the global dipole momentum (*i.e.* the coordinating *N*-benzimidazole atom is *trans* to the *N*-pyridine atom with respect to the inter-annular C–C bond and the *O*-amide atom is *trans* to the *N*-pyridine atom with respect to the C(py)–C(carbonyl) bond, Fig. 3).[18b,24] The adjacent pyridine and benzimidazole rings are not strictly co-planar (interplane angles: 33.6(1)° in **L4**^{b} and 13.58(4)–29.02(5)° in **L5**), while the two benzimidazole rings in **L5** are almost orthogonal (interplane angle 93.97(3)°). However, the latter angle is of very limited interest for characterizing the helicity induced by this famous diphenyl methane spacer.[22,25] We have therefore resorted to the detailed analysis of crooked lines proposed by Brewster[26] for the quantitative determination of the helicity index H (eqn (3)) associated with the specific organization of the five-carbon chain HC_{ar}–C_{ar}–CH_2–C_{ar}–$C_{ar}H$ in the spacer and numbered C13–C14–C20–C34–C33 in **L5** (Fig. 3b).

$$H = \frac{V}{V_{max}} = 6\sqrt{3}\pi\frac{L\cdot A}{D^3} \quad (3)$$

According to Brewster,[26] the five atoms are projected onto a plane perpendicular to the helical axis defined by the line passing through the two terminal atoms of the chain. This yields three possible geometrical figures: a line for non-helical organization, a quadrilateral for a regular helical crooked line and two triangles with a common summit for an amphiverse helix (Fig. 4a). The helicity index, computed with eqn (3), corresponds to the ratio of the volume enclosed by the crooked line (V) with respect to the maximum volume (V_{max}) produced when the subtended figure is a

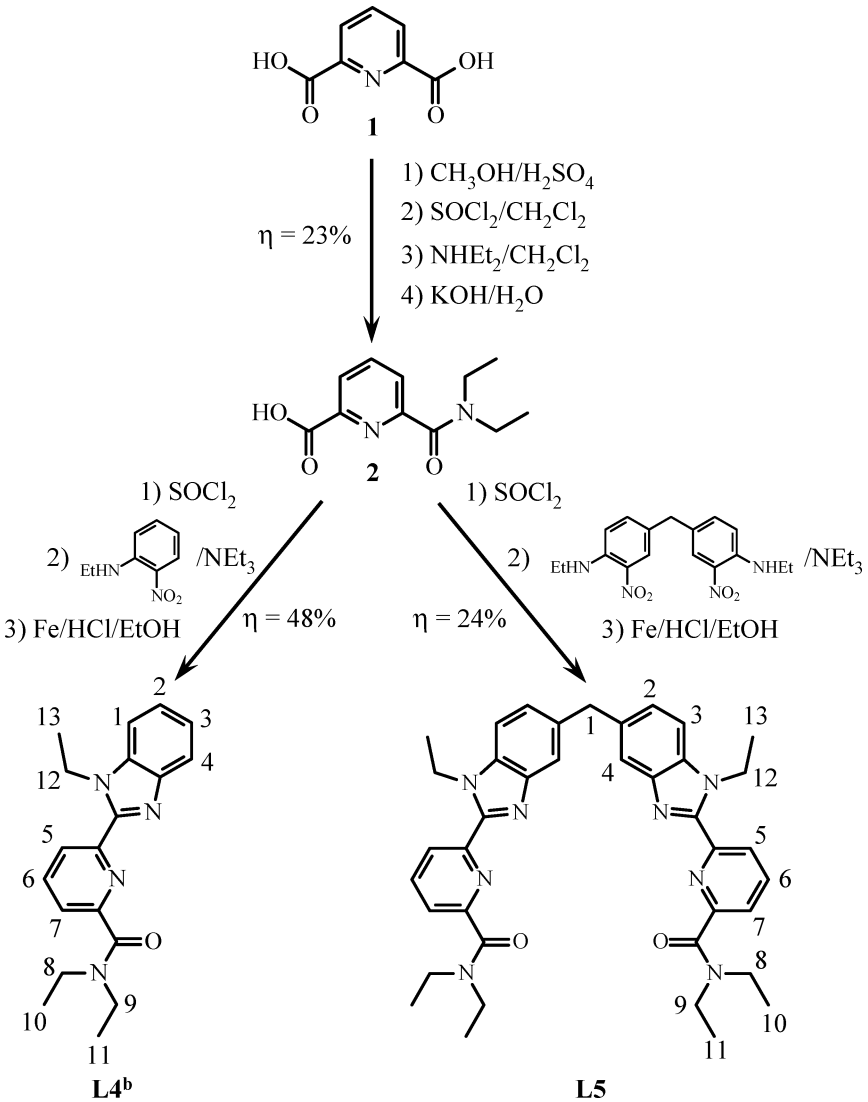

Scheme 2 Key synthons in the multi-step syntheses of **L4**^{b} and **L5** (numbering for NMR data is given).

circle (*L* is the end to end distance of the helix, *A* is the area of the subtended figure in the projection plane and *D* is the total length of the crooked line, Fig. 4a).[26] For **L5**, the subtended figure produced by the crooked line of the diphenyl methane spacer is diagnostic for an amphiverse helix with two helical domains possessing opposite helicities (Fig. 4b). The absolute sum of the two helical domains gives an absolute helicity index $H = 0.21$, but the difference of the two subtented areas eventually shows a net helicity of only $H = 0.15$. In other words, the diphenyl methane spacer in the free ligand **L5** possesses a poor global helicity resulting from the successive packing of short helical domains with opposite helicities.

Reaction of 1.0 equivalent of **L4**^{b} or **L5** with stoichiometric amounts (1.0 equiv. for **L4**^{b} and 2.0 equiv. for **L5**) of $Ln(NO_3)_3{\cdot}xH_2O$ (Ln = La, Eu, Gd, Tb, Lu, Y, x = 2–4) in acetonitrile, followed by precipitation with ^{t}Bu-methyl ether yields 75–85% of microcrystalline powders whose elemental analyses correspond to $[Ln(\mathbf{L4}^{b})(NO_3)_3]{\cdot}xH_2O$ (Ln = La, x = 2.5; Ln = Eu, x = 2; Ln = Gd, x = 2.5; Ln = Tb, x = 2.5; Ln = Lu, x = 1.5; Ln = Y, x = 1.5) and $[Ln_2(\mathbf{L5})(NO_3)_6]{\cdot}xH_2O$ (Ln = La, x = 3; Ln = Eu, x = 3.5; Ln = Gd, x = 4; Ln = Tb, x = 3.5; Ln = Lu, x = 6; Ln = Y, x = 4; Table S3, ESI).† Re-dissolution of the Eu complexes in acetonitrile or acetonitrile/propionitrile followed by slow evaporation yielded colourless X-ray quality prisms of $[Eu(\mathbf{L4}^{b})(NO_3)_3(CH_3CN)](CH_3CN)_2$ (**3**) and $[Eu_2(\mathbf{L5})(NO_3)_6(H_2O)_2](H_2O)_4(CH_3CH_2CN)_2$ (**4**). The crystal structure of **3** shows a ten-coordinated $[Eu(\mathbf{L4}^{b})(NO_3)_3(CH_3CN)]$ complex together with two interstitial solvent molecules. In the complex, the ligand **L4**^{b} adopts the *cis–cis* conformation required for its meridional tri-coordination to Eu^{III}, together with a slight helical twist of the benzimidazole–pyridine–carboxamide thread (interplane angles: benzimidazole–pyridine 11.3(1)° and pyridine–carboxamide 19.2(1)°, Fig. 5a and Tables S4 and S5, ESI).† The coordination sphere is completed with three bidentate nitrate anions and one solvent molecule as previously noticed for the analogous complexes $[Eu(\mathbf{L3}^{a})(NO_3)_3(CH_3OH)]$[18a] and $[Eu(\mathbf{L3}^{c})(NO_3)_3(CH_3CN)]$.[18b]

Except for the slightly shorter Eu–O(carboxamide) bond length in $[Eu(\mathbf{L4}^{b})(NO_3)_3(CH_3CN)]$, the coordination spheres in these three mononuclear complexes are almost superimposable (Fig. S2, ESI),† which is further substantiated by the calculation of very

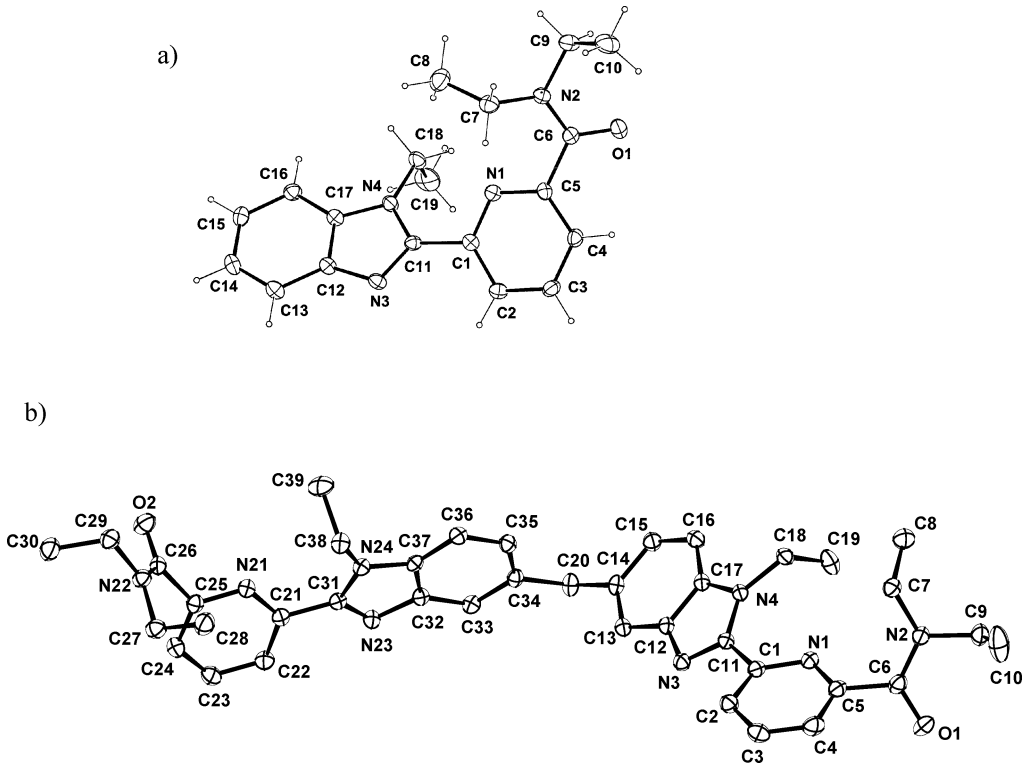

Fig. 3 Perspective views of the molecular structures of the ligands (a) **L4**^{b} and (b) **L5** with numbering schemes. Ellipsoids are represented at 50% probability level.

similar ionic radii $R_{Eu}^{CN=10}$,[27] bond valences v_{Eu_j}[28,29] and bond valence sums V_{Eu} (Table 1 and Tables S6–S8, ESI).† Moreover, the agreement found between the ionic radii and valence bond sums calculated in Table 1, with those expected for standard ten-coordinate Eu^{III} ($R_{Eu}^{CN=10}$ = 1.18 Å[30] and V_{Eu} = 3.00)[29] points to the lack of significant constraints produced by the coordination of the tridentate N_3 (in **L3**) or N_2O (in **L4**^{b}) units in the nitrato complexes. Finally, in the crystal of **3**, a single weak intermolecular π-stacking interaction can be detected between the benzimidazole rings of two adjacent [Eu(**L4**^{b})$(NO_3)_3(CH_3CN)$] complexes related by a centre of inversion (interplane angle 0°, interplane distance 3.46(1) Å).

Interestingly, the extended binuclear complex [Eu_2(**L5**)$(NO_3)_6(H_2O)_2$] crystallizes in the *C*2/*c* space group (monoclinic) with the bridging methylene carbon of the diphenyl methane spacer C20 located on a two-fold axis (Fig. 5b). Comparisons with the mononuclear analogue are thus simplified and the metallic coordination sphere of the asymmetrical unit of [Eu_2(**L5**)$(NO_3)_6(H_2O)_2$] can be almost perfectly superimposed with that of [Eu(**L4**^{b})$(NO_3)_3(CH_3CN)$], except for the replacement of an acetonitrile solvent molecule with water (Fig. S3, ESI).† Consequently, the metric of the coordination spheres in [Eu_2(**L5**)$(NO_3)_6(H_2O)_2$] (Tables S10, ESI),† the associated interplanar angles (Table S11, ESI)† and the bond valence sums (Table 1 and Table S9, ESI)† are comparable with those found in the mononuclear analogue. The only significant difference concerns the existence of a network of hydrogen bonds in the crystal of **4** involving coordinated and interstitial water molecules, which produces infinite zig-zag chains of complexes along the [1 0 1] direction (Fig. S4, ESI).† The benzimidazole rings in [Eu_2(**L5**)$(NO_3)_6(H_2O)_2$] are further involved in weak intermolecular π-stacking interactions operating about centres of inversion (interplanar angle 0°, interplanar distances 3.32 Å), which produce a compact packing of the zig-zag chains of complexes in the solid state (Fig. S5, ESI).† The Eu^{III} atoms are regularly spaced along these chains (intramolecular $Eu1\cdots Eu1_{(1-x,y,1/2-z)}$ = 8.564(1) Å, intermolecular $Eu1\cdots Eu1_{(3/2-x,\,3/2-y,1-z)}$ = 8.720(1) Å) with intermetallic distances comparable to Tb···Tb = 9.06(3) Å found in the binuclear triple-stranded helicate [Tb_2(**L5**$)_3$]$(ClO_4)_6$.[22a] The symmetrical quadrilateral produced by the subtended figure of the projected crooked line C18–C17–C20–C17′–C18′ (Fig. 4c), indicates a regular helical organization of the diphenylmethane spacer in [Eu_2(**L5**)$(NO_3)_6(H_2O)_2$], which can be thus considered as a binuclear single-stranded complex with an index of helicity of H = 0.76 (eqn (3)). Applying eqn (3) for the three strands of the triple-stranded helicate [Tb_2(**L5**$)_3$]$(ClO_4)_6$ yields H = 0.58, 0.67 and 0.73 (average 0.66), which points to a similar helical organization of the bis-tridentate ligands **L5** in the single-stranded and in the triple-stranded helicates.

Structures of the ligands L4^{b} and L5, and of their complexes [Ln(L4^{b})$(NO_3)_3$]·$x$$H_2O$ and [Ln_2(L5)$(NO_3)_6$]·$x$$H_2O$ (Ln = La, Eu, Lu, Y) in acetonitrile

^{1}H NMR titrations of the C_s-symmetrical ligand **L4**^{b} (10 mol dm^{-3}) with $Ln(NO_3)_3\cdot xH_2O$ (Ln = La, Eu, Lu, Y, x = 2–4) in CD_3CN show the formation of a single complex, in which the C_s symmetry is maintained (all methylene protons are enantiotopic, Fig. S6, ESI).† The detection of a significant nuclear Overhauser effect (NOE) between H5 and H12 upon reaction of **L4**^{b} with $Ln(NO_3)_3$

Table 1 Ionic radii ($R_{Eu}^{CN=10}$/Å),[a] average bond valences ($v_{Eu,j}$)[b] and bond valence sum (V_{Eu})[c] in the crystal structures of [Eu(**L3**[a])$(NO_3)_3(CH_3OH)$],[18a] [Eu(**L3**[e])$(NO_3)_3(CH_3CN)$],[18b] [Eu(**L4**[b])$(NO_3)_3(CH_3CN)$] (**3**) and $[Eu_2(\mathbf{L5})(NO_3)_6(H_2O)_2]$ (**4**)

	[Eu(**L3**[a])$(NO_3)_3(CH_3OH)$]	[Eu(**L3**[e])$(NO_3)_3(CH_3CN)$]	[Eu(**L4**[b])$(NO_3)_3(CH_3CN)$]	$[Eu_2(\mathbf{L5})(NO_3)_6(H_2O)_2]$
$R_{Eu}^{CN=10}$ [a]	1.17	1.16	1.17	1.16
v_{Eu-Npy} [b]	0.30	0.29	0.28	0.28
$v_{Eu-Nbzim}$ [b]	0.39(4)	0.39(3)	0.36	0.39
$v_{Eu-Oamide}$ [b]	—	—	0.41	0.42
$v_{Eu-ONO2}$ [b]	0.28(5)	0.28(4)	0.27(2)	0.26(3)
$v_{Eu-solvent}$ [b]	0.29	0.33	0.31	0.34
V_{Eu} [c]	3.04	3.06	2.98	2.98

[a] Ionic radius for ten-coordinate Eu^{III} calculated by using Shannon's definition with $r(N) = 1.46$ Å, $r(O) = 1.35$ Å and r(O-nitrate) = 1.31 Å.[27] [b] $v_{Eu,j} = e^{[(R_{Eu,j} - d_{Eu,j})/b]}$ with valence bond parameters $R_{Eu,N}$ and $R_{Eu,O}$ taken from ref. 29 and $b = 0.37$ Å.[28] [c] $V_{Eu} = \sum_j v_{Eu,j}$.[28]

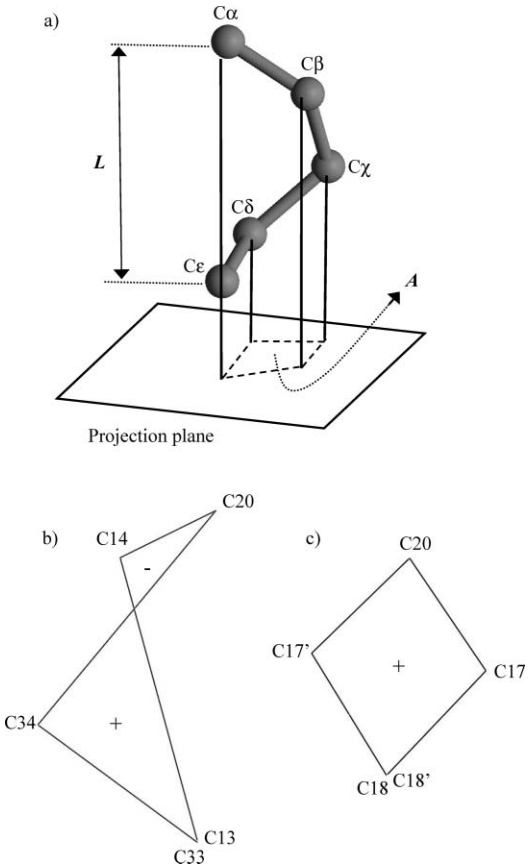

Fig. 4 (a) Analysis of the helicity of a five-atoms crooked line proposed by Brewster (*L* is the end to end distance of the helix, *A* is the area of the subtended figure in the projection plane and *D* is the total length of the crooked line).[26] Subtented geometrical figures obtained in the projection plane for (b) **L5** and (c) $[Eu_2(\mathbf{L5})(NO_3)_6(H_2O)_2]$.

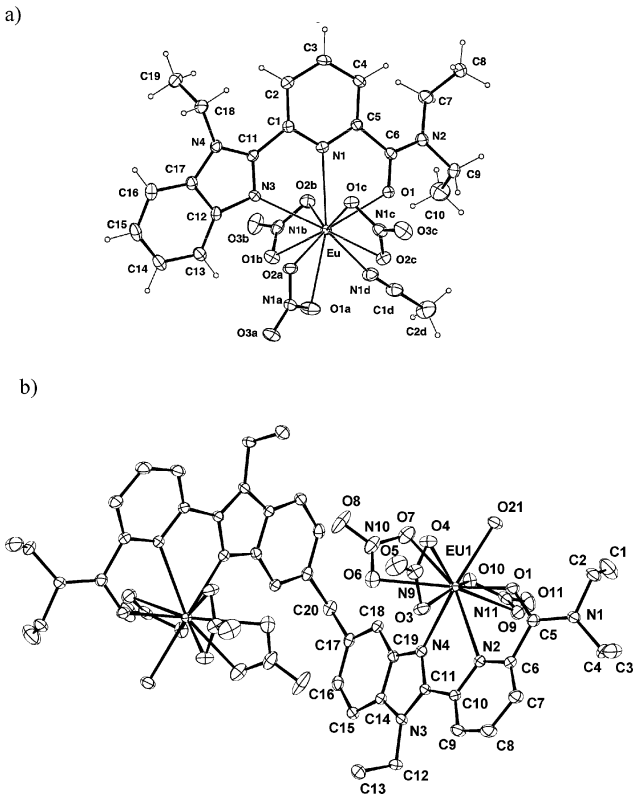

Fig. 5 Perspective views with numbering schemes of the molecular structures of the complexes (a) [Eu(**L4**[b])$(NO_3)_3(CH_3CN)$] in the crystal structure of **3** and (b) $[Eu_2(\mathbf{L5})(NO_3)_6(H_2O)_2]$ in the crystal structure of **4**. Ellipsoids are represented at 50% probability level.

(Ln = La, Eu, Lu, Y, numbering in Scheme 2) confirms the *trans–trans* to *cis–cis* conformational change of the tridentate N_2O binding units resulting from the complexation of the metal, while the noticeable downfield shift of proton H6 in the diamagnetic complexes ($\Delta\delta = 0.35$ ppm in La, $\Delta\delta = 0.40$ ppm in Lu and $\Delta\delta =$ 0.43 ppm in Y, Table S12 and Fig. S6, ESI),† is diagnostic for the interaction of the pyridine ring with the cation.[31] Surprisingly, the ^{1}H NMR spectra display broadened signals for the exact stoichiometric ratio Ln:**L4**[b] = 1.0, and resolution is significantly improved when using an excess of metal (Lu:**L4**[b] ≥ 1.3 for Ln = Lu, but Ln:**L4**[b] ≥ 3.0 for larger lanthanides such as Ln = Eu, La). On the other hand, neither variable-temperature ^{1}H NMR data, nor addition of an excess of NBu_4NO_3 in solution, nor an increase in the total ligand concentration improve resolution, and we conclude that the broadening of the NMR signals can be assigned to slow intermolecular on/off ligand complexation processes on the NMR time scale. In agreement with the expected increase in both stability and kinetic inertness with smaller lanthanides,[32] the broadening is maximum for Ln = La^{III} and becomes negligible

in excess of metal because of the reduced mole fraction of uncomplexed ligand (Fig. S6b and S6c, ESI).†[33] Moreover, even in excess of metal, the NMR signals of the benzimidazole protons H1–H4 in [La(**L4**^{b})$(NO_3)_3$] remains large (Fig. S6c, ESI),† which further suggests the operation of slow intramolecular partial on/off decomplexation of the benzimidazole side arms with the larger lanthanides in solution (*i.e.* a hemilabile benzimidazole side arms).

Since the reactions of $Ln(NO_3)_3$ with tridentate aromatic ligands mainly produce neutral species in acetonitrile,[18,19,34] ESI-MS is of limited interest for investigating the speciation of the complexes in solution. We have therefore resorted to diffusion-ordered spectroscopy (DOSY-NMR) for the determination of the translational self-diffusion coefficient D for the ligands and for their complexes in order to unravel the size, the shape and the stoichiometries of the complexes formed in solution. For a hard spherical particle of dimension much larger than the molecules of solvent considered as a continuum, the Stokes–Einstein eqn (4) relates the translational diffusion coefficient with the temperature (T), the viscosity ($\eta = 3.65 \times 10^{-4}$ kg m^{-1} s^{-1} for acetonitrile at 293 K) and the hydrodynamic radius r_H.

$$D = \frac{kT}{6\pi\eta r_H} \quad (4)$$

When the size of the particle x approaches that of the solvent molecules, the frictional coefficient (*i.e.* the denominator of eqn (4)), must be corrected by a factor derived from microfrictional theory[36] and semi-empirically improved by Chen,[37] which eventually yields eqn (5), whereby r_{solv} is the hydrodynamic radius of the solvent.

$$D_x = \left(\frac{kT}{6\pi\eta r_H^x}\right)\left(1 + 0.695\left(r_{solv}/r_H^x\right)^{2.234}\right) \quad (5)$$

In parallel, the spherical equivalent radius of a molecule x can be calculated from its partial specific volume ($v_x = (d_x)^{-1}$ in cm^3 g^{-1}) and its molecular weight (M_x in g mol^{-1}) by using eqn (4), in which N_A is Avogadro's constant.[35,38]

$$r_{eq}^x = \sqrt[3]{\frac{3M_x v_x}{4\pi N_A}} = \sqrt[3]{\frac{3V_x^{mol}}{4\pi}} \quad (6)$$

It is worth noting that $M_x v_x / N_A$ simply corresponds to the volume of the molecule (V_x^{mol}) not accessible to the solvent molecules in solution, which can be estimated by using the Connolly volume (*i.e.* the volume limited by the Connolly surface built around the molecule).[39] If the molecule is spherical, we expect $r_{eq}^x \cong r_H^x$, but these two parameters are related by a shape factor (eqn (7)) for non-spherical molecules.[40] For the rough treatment proposed here, molecules are considered as ellipsoids characterized by the geometrical factor $p = a/b$, whereby a is the semi-major axis and b is the semi-minor axis of the ellipsoids with $a > b$. The associated shape factors are then given by eqn (8) for prolate (*i.e.* cigar-like ellipsoids with two short and one long axes) and by eqn (9) for oblate (*i.e.* disk-like ellipsoids with two long and one short axes).[41]

$$r_H^x = r_{eq}^x / f(p) \quad (7)$$

$$f(p) = p^{1/3}(p^2 - 1)^{-1/2} \ln[p + (p^2 - 1)^{1/2}] \quad (8)$$

$$f(p) = p^{1/3}(p^2 - 1)^{-1/2} \arctan[(1 - p^2)^{1/2} p^{-1}] \quad (9)$$

Table 2 Experimental translational self-diffusion coefficients (D_x) and Connolly volumes (V_x^{mol}),[a] and calculated equivalent radii (r_{eq}^x, eqn 6), hydrodynamic radii (r_H^x, eqn (5)), shape functions ($f(p)$, eqn (7)) and geometrical factors for prolate ellipsoids (p, eqn (8)) for **L4**^{b}, **L5** and their complexes [Ln(**L4**^{b})$(NO_3)_3$] and [Ln_2(**L5**)$(NO_3)_6$] in CD_3CN at 293 K (Ln = La, Eu, Lu)

Compds	D_x/m^{2}s^{-1}	V_x^{mol}/Å^3	r_{eq}^x/Å	r_H^x/Å	$f(p)$	p
L4^b	$1.65(6) \times 10^{-9}$	298	4.1	3.9(2)	1.0	1.0
[La(**L4**^{b})$(NO_3)_3$]	$1.28(4) \times 10^{-9}$	440	4.7	4.9(2)	1.0	1.0
[Eu(**L4**^{b})$(NO_3)_3$]	$1.30(5) \times 10^{-9}$	440	4.7	4.8(1)	0.96	1.8
[Lu(**L4**^{b})$(NO_3)_3$]	$1.30(3) \times 10^{-9}$	440	4.7	4.9(1)	0.98	1.5
L5	$1.20(3) \times 10^{-9}$	611	5.2	5.1(1)	0.96	1.8
[La_2(**L5**)$(NO_3)_6$]	$8.55(9) \times 10^{-10}$	972	6.1	7.1(1)	0.86	3.7
[Eu_2(**L5**)$(NO_3)_6$]	$8.74(9) \times 10^{-10}$	972	6.1	6.9(1)	0.88	3.4
[Lu_2(**L5**)$(NO_3)_6$]	$8.79(4) \times 10^{-10}$	972	6.1	6.91(4)	0.88	3.4

[a] The Connolly volumes are obtained from the building of the Connolly surface around the molecular structures of ligands and complexes observed in their crystal structure and by using a probe radius of 2.0 Å for modelling acetonitrile solvent molecule ($V_{CH3CN} = 36.3$ Å^3).

The experimental translational diffusion coefficients D_x obtained by DOSY-NMR for **L4**^{b} and for its complexes [Ln(**L4**^{b})$(NO_3)_3$] in acetonitrile (293 K), together with the equivalent spherical radii r_{eq}^x calculated with eqn (6) and using the Connolly volume (V_x^{mol}) estimated from the molecular structures found in the crystal structures of **L4**^{b} and [Eu(**L4**^{b})$(NO_3)_3(CH_3CN)$] are collected in Table 2.

Taking $r_{solv}/r_H^x = D_x/D_{solv}$ (eqn (4)) with $D_{CD2HCN} = D_{solv} = 4.63 \times 10^{-9}$ m^2 s^{-1} measured with our experimental setup (DOSY-NMR, 293 K) allows the calculation of r_H^x (eqn (5)), which can be then compared with r_{eq}^x to obtain the shape factor $f(p)$ (eqn (7)) and the final geometrical factor p by fitting eqn (8) for prolate ellipsoids (Table 2). For **L4**^{b}, the experimental hydrodynamic radius strictly matches r_{eq}^x thus leading to a unit geometrical shape factor. For the mononuclear complexes [Ln(**L4**^{b})$(NO_3)_3$], r_{eq}^x is only slightly smaller than r_H^x (at the limit of the experimental errors), which results in shape factors also close to unity (eqn (7), $f(p) = 0.96$–0.98). Application of eqn (8) for prolate ellipsoids gives an approximate geometrical factor of $p \approx 1.5$ in fair agreement with the semi-major $a/2 = 6.7$ Å and semi-minor $b/2 = 5.0$ Å axes estimated for the ellipsoids ($p = a/b = 1.3$) enveloping the molecular structure of the complex [Eu(**L4**^{b})$(NO_3)_3(CH_3CN)$] in the solid state (Fig. 5a). We conclude that **L4**^{b} and its mononuclear complexes behave in solution as pseudo-spherical objects with metric dimensions very similar to those found in the solid state. This unambiguously confirms the exclusive formation of [Ln(**L4**^{b})$(NO_3)_3$] in solution with no trace of dimerization processes, a behaviour in strong contrast with the systematic detection of mixture of 1 : 1 and 2 : 2 complexes in slow exchange on the NMR time scale with the tridentate N_3 donors in [Ln(**L3**)$(NO_3)_3$].[18] The case of the extended bis-tridentate ligand **L5** is more informative since its ^{1}H NMR spectrum in solution is diagnostic for an average C_{2v}-symmetrical conformation (Fig. 6a, two equivalent tridentate units combined with A_2 spin systems (enantiotopic protons) for the methylene probes H1, H8, H9 and H12) only compatible with a planar arrangement of the diphenyl methane spacer (distal or proximal) with absolute zero helicity on the NMR time scale (Fig. S7, ESI).†

The minor deviation of r_H^x, computed with eqn (5) by using the translational diffusion coefficient of **L5**, from r_{eq}^x calculated

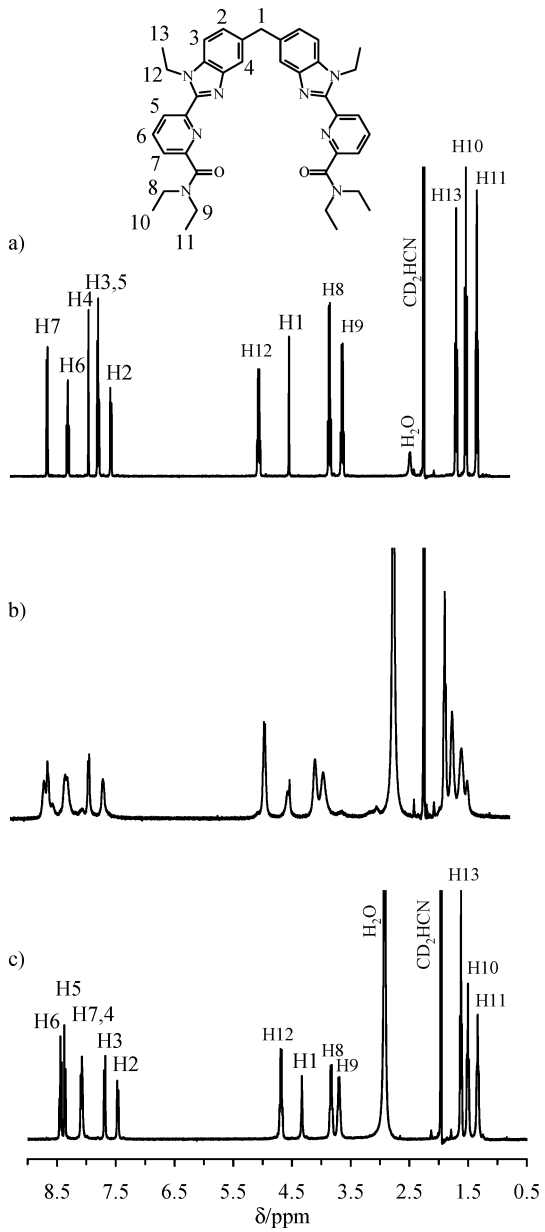

Fig. 6 ^{1}H NMR spectra obtained upon titration of **L5** with $Lu(NO_3)_3{\cdot}2H_2O$ for (a) Lu–**L5** = 0 : 1, (b) Lu–**L5** = 2 : 1 and (c) Lu–**L5** = 3 : 1.

from the Connolly volume (eqn (6), Table 2) points to a rather compact and pseudo-spherical shape for the free ligand in solution ($f(p) \approx 1$, Table 2), which is tentatively ascribed to a proximal conformation of the coordinating nitrogen atoms of the benzimidazole units in the free ligand in solution (Fig. S7a, ESI).† Upon titration with $Ln(NO_3)_3{\cdot}xH_2O$ (Ln = La, Eu, Lu,; x = 2–4) in CD_3CN, the observed significant broadening of all ^{1}H NMR signals resolves into a single species for Ln:**L5** ≥ 2.0, which displays C_{2v}-symmetry (enantiotopic methylene probes) in line with the planar arrangement of the diphenylmethane spacer (Fig. 6b and c, and Table S12, ESI).† As previously noticed with the mononuclear analogues, intermolecular on-off decomplexation of the tridentate binding units occurring at an intermediate rate on the NMR time scale requires an excess of metal for minimizing the effect of the exchange process on the NMR spectra (Fig. 6c).[33] The NOE effects detected between H5–H12 combined with the downfield shift of H6 (Table S12, ESI)† are diagnostic for the meridional tri-coordination of the tridentate benzimidazole-pyridine-carboxamide units to $Ln(NO_3)_3$. DOSY-NMR data provide translational diffusion coefficients, from which the calculated hydrodynamic radii (r_H^x, eqn (5)) now significantly deviate from the equivalent spherical radii estimated from the molecular volume (r_{eq}^x, eqn (6), Table 2). The resulting shape factors $f(p)$ = 0.86–0.88 obtained for $[Ln_2(\mathbf{L5})(NO_3)_6]$ (eqn (7)) indicate a significant deviation from spherical behaviour with p = 3.4–3.7. Taking the crystal structure of the single-stranded helical complex $[Eu_2(\mathbf{L5})(NO_3)_6(H_2O)_2]$ as a starting point (Fig. 5b), we can estimate major $a \approx 19.3$ Å and minor $b \approx 8.9$ Å axes yielding $p = a/b = 2.2$ in poor agreement with the solution data (Fig. 7a). The planarization of the diphenyl methane spacer on the NMR time scale, which is required by the C_{2v}-symmetry observed for $[Ln_2(\mathbf{L5})(NO_3)_6]$ in solution, is only compatible with a distal arrangement of the spacer for obvious steric constraints (Fig. S7c, ESI).† Consequently, the intramolecular contact Ln ··· Ln increases (12.3 Å) together with the geometrical factor $p = a/b \approx 25.4/7.5 = 3.4$, which is now in fair agreement with NMR data (Fig. 7b). More sophisticated shape analysis based on translational diffusion coefficients are available for cylinders[42] and dumbbell,[43] but their application is only justified with rather rigid structures in solution such as cyclodextrins[44] for which one geometrical parameter (diameter or length) is fixed, a condition not met by our flexible single-stranded complex. We can thus safely conclude from the NMR data that the complexes $[Ln(\mathbf{L4}^b)(NO_3)_3]$ and $[Ln_2(\mathbf{L5})(NO_3)_6]$ are the only assembled species formed in acetonitrile for Ln:$\mathbf{L4}^b$ ≥ 1.0 and Ln:**L5** ≥ 2.0, respectively. Moreover, the mononuclear complexes retain their pseudo-spherical globular shapes on the NMR time

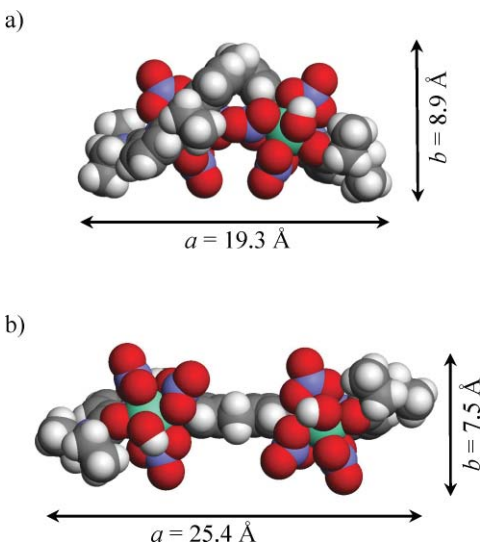

Fig. 7 CPK representations of $[Eu_2(\mathbf{L5})(NO_3)_6(H_2O)_2]$ (a) in the crystal structure of **4** and (b) in solution with a planar C_{2v}-symmetrical conformation (distal) of the diphenylmethane spacer (built from the crystal structure of **4** except for the two dihedral angles C18–C17–C20–C17′ and C17–C20–C17′–C18′, which are set to zero). The approximate magnitude of the major (z) and minor (x) axes of the prolate ellipsoids are shown.

scale, while the binuclear complexes adopt extended C_{2v}-symmetry conformations of the diphenyl spacer with absolute zero helicity.

Thermodynamics of the complexation of the ligands L4[b] and L5 with $Ln(NO_3)_3$ (Ln = La, Eu, Lu, Y) in acetonitrile

The *trans–trans* toward *cis–cis* conformational change of the tridentate binding unit accompanying the complexation of the polyaromatic ligands **L4**[b] and **L5** to $Ln(NO_3)_3$ alters the envelope of the ligand-centred $n \rightarrow \pi^*$ and $\pi \rightarrow \pi^*$ transitions (Fig. S8, ESI),† which allows the quantitative evaluation of the coordination process by using spectrophotometric titrations (Fig. 8).[45]

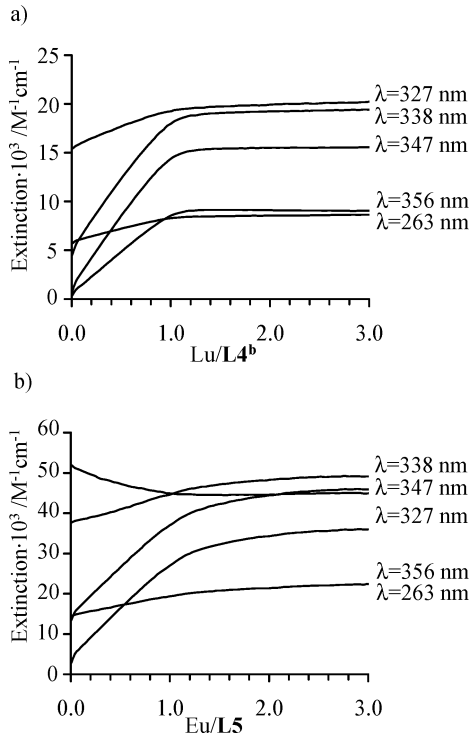

Fig. 8 Variation of molar extinction at 5 different wavelengths observed during the spectrophotometric titrations of (a) **L4**[b] with $Lu(NO_3)_3 \cdot 2H_2O$ and (b) **L5** with $Eu(NO_3)_3 \cdot 3H_2O$ (293 K, CH_3CN, total ligand concentration: 10^{-4} mol dm^3).

The observation of an isosbestic point at 322 nm (Fig. S8a, ESI)† combined with a smooth end point for Ln:**L4**[b] = 1.0 (Fig. 8a) confirms the exclusive formation of $[Ln(\mathbf{L4^b})(NO_3)_3]$ in acetonitrile. For **L5**, the lack of isosbestic points together with the detection of two smooth end points for Ln:**L5** = 1.0 and 2.0 imply the successive formation of $[Ln(\mathbf{L5})(NO_3)_3]$ and $[Ln_2(\mathbf{L5})(NO_3)_6]$ complexes (Figs. 8b and S8b, ESI).† Factor analyses[46] further support the formation in solution of two absorbing species with **L4**[b], respectively, three absorbing species with **L5**. The global spectrophotometric data can be then fitted to the three macroscopic equilibria (eqn (10)–(12)) by using non-linear least-squares techniques (Table 3).[47]

$$Ln(NO_3)_3 + \mathbf{L4^b} \rightleftharpoons [Ln(\mathbf{L4^b})(NO_3)_3] \quad \beta_{1,1}^{Ln,L4b} \tag{10}$$

$$Ln(NO_3)_3 + \mathbf{L5} \rightleftharpoons [Ln(\mathbf{L5})(NO_3)_3] \quad \beta_{1,1}^{Ln,L5} \tag{11}$$

$$2\,Ln(NO_3)_3 + \mathbf{L5} \rightleftharpoons [Ln_2(\mathbf{L5})(NO_3)_6] \quad \beta_{2,1}^{Ln,L5} \tag{12}$$

Application of the site binding model (eqn (2)) to each macroscopic formation constants (eqn (10–12)) provides three equations for each lanthanide (eqn (13–15)), in which (i) the statistical factors $\omega_{m,n}^{chiral} \cdot \omega_{m,n}^{Ln,L}$ are obtained by using the method of symmetry numbers (Fig. S9, ESI),†[48] (ii) $f_{N2O}^{Ln,L}$ represents the absolute affinity of the N_2O tridentate binding unit of each ligand for $Ln(NO_3)_3$ and (iii) $u^{Ln,Ln} = e^{-\Delta E^{Ln,Ln}/RT}$ is the Boltzmann factor measuring the intramolecular intermetallic interaction operating in the binuclear $[Ln_2(\mathbf{L5})(NO_3)_6]$ complexes.

$$\beta_{1,1}^{Ln,L4b} = \omega_{1,1}^{chiral} \cdot \omega_{1,1}^{Ln,L4b} \cdot f_{N2O}^{Ln,L4b} = 3 \cdot f_{N2O}^{Ln,L4b} \tag{13}$$

$$\beta_{1,1}^{Ln,L5} = \omega_{1,1}^{chiral} \cdot \omega_{1,1}^{Ln,L5} \cdot f_{N2O}^{Ln,L5} = 6 \cdot f_{N2O}^{Ln,L5} \tag{14}$$

$$\beta_{2,1}^{Ln,L5} = \omega_{2,1}^{chiral} \cdot \omega_{2,1}^{Ln,L5} \cdot \left(f_{N2O}^{Ln,L5}\right)^2 \cdot u^{Ln,Ln} = 9 \cdot \left(f_{N2O}^{Ln,L5}\right)^2 \cdot u^{Ln,Ln} \tag{15}$$

A rapid inspection of the thermodynamic data collected in Table 3 shows that $\beta_{1,1}^{Ln,L5} < \beta_{1,1}^{Ln,L4b}$ despite the twofold increases of the statistical factors reflecting the two possibilities for $Ln(NO_3)_3$ to bind a tridentate binding unit in **L5** (eqn (14)), while only a single binding site is available for **L4**[b] (eqn (13)). This implies that the absolute affinities are different for the tridentate N_2O binding unit in the two ligands ($f_{N2O}^{Ln,L5} < f_{N2O}^{Ln,L4b}$), a trend which can be tentatively assigned to the substitution of the benzimidazole ring with the methylene spacer in **L5** and/or to some different solvation processes accompanying the complexation processes of the two ligands. In these conditions, the fit of eqn (13)–(15) requires the physically debatable use of three microscopic

Table 3 Experimental and calculated[a] cumulative thermodynamic macroconstants obtained from the spectrophotometric titrations of **L4**[b] and **L5** with $Ln(NO_3)_3 \cdot xH_2O$ in acetonitrile (293 K, Ln = La, Eu, Lu, Y, x = 2–4)

Ligand	Ln^{III}	$R_{Ln}^{CN=9}$/Å [b]	$\log(\beta_{1,1}^{Ln,L})$	$\log(\beta_{2,1}^{Ln,L})$	$\log(\beta_{1,1}^{Ln,L})_{calcd}$ [a]	$\log(\beta_{2,1}^{Ln,L})_{calcd}$ [a]
L4[b]	La	1.216	5.77(6)	—	5.28	—
L4[b]	Eu	1.120	5.27(9)	—	5.23	—
L4[b]	Y	1.075	5.99(9)	—	5.69	—
L4[b]	Lu	1.032	6.06(9)	—	5.77	—
L5	La	1.216	5.09(9)	9.20(8)	5.58	9.20
L5	Eu	1.120	5.49(4)	9.42(6)	5.53	9.42
L5	Y	1.075	5.69(8)	10.12(9)	5.99	10.12
L5	Lu	1.032	5.79(9)	10.36(9)	6.09	10.36

[a] Calculated with eqns (13)–(15) and the microscopic parameters taken from Table S13. [b] Ionic radii for nine-coordinate lanthanides.[27a]

Table 4 Fitted microscopic thermodynamic parameters for $[Ln(\mathbf{L4^b})(NO_3)_3]$ and $[Ln_m(\mathbf{L5})(NO_3)_6]$ (m = 1, 2) in acetonitrile (eqn (13)–(15) using two different affinity parameters $f_{N2O}^{Ln,L4b}$ and $f_{N2O}^{Ln,L5}$, Ln = La, Eu, Lu, Y, 293 K)[a]

Ln^{III}	$\log\left(f_{N2O}^{Ln,L4b}\right)$	$\Delta G_{N2O}^{Ln,L4b}$/kJ mol^{-1}	$\log\left(f_{N2O}^{Ln,L5}\right)$	$\Delta G_{N2O}^{Ln,L5}$/kJ mol^{-1}	$\log(u^{Ln,Ln})$	$\Delta E^{Ln,Ln}$/kJ mol^{-1}
La	5.29	−30.2	4.31	−24.6	−0.38	2.2
Eu	4.79	−27.3	4.71	−26.9	−0.96	5.5
Y	5.51	−31.4	4.91	−28.0	−0.66	3.8
Lu	5.58	−31.8	5.01	−28.6	−0.62	3.5

[a] Since three parameters are fitted to the three eqn (13)–(15), there are no uncertainties.

parameters ($f_{N2O}^{Ln,L4b}$, $f_{N2O}^{Ln,L5}$ and $u^{Ln,Ln}$) for fitting three experimental stability constants, which obviously yields no uncertainties (Table 4).

We can however globally analyze the trends obtained for these microscopic parameters. Firstly, the absolute affinities increase with decreasing ionic radii, in agreement with the classical electrostatic model developed for polar solvents.[32a] The free energies of connection of $Ln(NO_3)_3$ to the tridentate N_2O binding unit, which reflect the desolvation of the two partners followed by their intermolecular binding, amount to $-32 < \Delta G_{N2O}^{Ln,L4b} = -RT\ln\left(f_{N2O}^{Ln,L4b}\right) < -27$ kJ mol^{-1} and $-29 < \Delta G_{N2O}^{Ln,L5} = -RT\ln\left(f_{N2O}^{Ln,L5}\right) < -24$ kJ mol^{-1}. These values are comparable to $\Delta G_{N2O}^{Lu,L5} = -31(1)$ kJ mol^{-1} previously estimated for the binding of the same tridentate unit in the same solvent, but to Eu^{3+} in the triple-stranded helicates $[Eu_2(\mathbf{L5})_3]^{6+}$ (Eu^{3+} is obtained from $Eu(O_3SCF_3)_3$).[15] According to the different effective charge borne by the metal in Ln^{3+} and in $Ln(NO_3)_3$, we deduce that solvation processes play a major role in the global stability of these complexes and they probably overcome the decrease in affinity predicted for $Ln(NO_3)_3$ on simple point charge electrostatic bases. The intermetallic interaction is systematically repulsive with an average value of $\Delta E^{Ln,Ln} = 3.8(1.4)$ kJ mol^{-1}, which implies the operation of an anti-cooperative process for the successive binding of two $Ln(NO_3)_3$ to **L5**.[12] Interestingly, its magnitude is also comparable to that obtained in triple-stranded helicates $\Delta E^{Lu,Lu} = 10(4)$ kJ mol^{-1},[16] despite (i) the increased intermetallic distance (9 Å in $[Ln_2(\mathbf{L5})_3]^{6+}$ and 12.3 Å in $[Ln_2(\mathbf{L5})(NO_3)_6]$) and (ii) the charge compensation brought by the bound nitrate anions. Again, this points to the prominent contribution of solvation processes to the assembly process.[15] For the neutral nitrato complexes, the simplistic electrostatic point charge arguments based on Coulomb and Born equations previously used for $[Ln_2(\mathbf{L5})_3]^{6+}$[15,16] cannot be invoked, and more detailed calculations involving neutral polar molecules in a dielectric continuum must be considered.[49] It is however remarkable, and slightly disappointing, that the successive fixation of both neutral $Ln(NO_3)_3$ and charged Ln^{3+} metals to **L5** produces comparable and weakly repulsive intermetallic interactions. In an attempt to obtain rough, but physically meaningful microscopic parameters, we have fitted eqn (13)–(15) with only two parameters, one average absolute metal–ligand affinity $f_{N2O}^{Ln,L5}$ and one intermetallic interaction $\Delta E^{Ln,Ln}$ (Table S13, ESI).† Obviously, the uncertainties are rather large and the experimental data measured for $\beta_{1,1}^{Ln,L4b}$ and $\beta_{1,1}^{Ln,L5}$ are poorly reproduced (Table 3), but we still notice the operation of a strictly anti-cooperative process along the complete lanthanide series.

Photophysical properties of the ligands L4^b and L5, and of their complexes $[Ln(\mathbf{L4^b})(NO_3)_3]\cdot xH_2O$ and $[Ln_2(\mathbf{L5})(NO_3)_6]\cdot xH_2O$ (Ln = Eu, Gd, Tb)

The electronic absorption spectra of the ligands in acetonitrile display a broad band centered at 31 200 cm^{-1} ($\varepsilon \approx$ 22 000–25 000 M^{-1}cm^{-1} per tridentate binding unit, Table 5, Fig. S8, ESI),† which can be assigned to the envelope of the $n \rightarrow \pi^*$ and $\pi \rightarrow \pi^*$ transitions in analogy with closely related characteristics theoretically established for the tridentate 2,6-bis(benzimidazol-2-yl)pyridine units in **L3**^{a} (31 150 cm^{-1}, ε = 32 000 M^{-1}cm^{-1}).[18,45,50] The larger molar extinction coefficient in **L3**^{a} results from the more extended aromatic structure. Excitation trough the ligand-centered $\pi \rightarrow \pi^*$ transitions in **L4**^{b} or in **L5** ($\tilde{\nu}_{exc}$ = 32 260 cm^{-1}, solid state, 77K) produces strong and structured fluorescence at *ca.* 27 000 cm^{-1} (0–0 phonon), whose short lifetime ($\tau < 100$ ns) is diagnostic for emission arising from the $^1\pi\pi^*$ level (Fig. S10a and S11a, ESI).† Despite the introduction of various delays (0.1–1 ms) in time-resolved spectra, no phosphorescence could be detected for the flexible free ligands. Upon complexation to $Ln(NO_3)_3$ in the complexes $[Ln(\mathbf{L4^b})(NO_3)_6]$ and $[Ln_2(\mathbf{L5})(NO_3)_6]$ (Ln = Eu, Gd, Tb), we observe a 500–750 cm^{-1} red-shift of the ligand-centred absorption band, which has been exploited for spectrophotometric titrations (Fig. S8, ESI).† Since the excited metal-centered levels of Gd^{III} lie at too high energy (≥ 32 000 cm^{-1})[51] for being accessible for efficient intramolecular energy transfer from the ligand-centred $^1\pi\pi^*$ or $^3\pi\pi^*$ levels, the emission spectra of $[Gd(\mathbf{L4^b})(NO_3)_6]$ and $[Gd_2(\mathbf{L5})(NO_3)_6]$ indeed probes the energy of the latter levels after complexation, which are indeed located close in energy to those found in the free ligand (Table 5, Fig. S10b and S11b, ESI).† However, the concomitant operation of spin–orbit coupling and Coulomb interactions between the electrons of the ligands and those of the paramagnetic gadolinium metal mix the ligand-centred singlet and triplet wavefunctions,[52] a phenomenon which considerably increases both intersystem crossing (ISC) and the oscillator strength of the spin-forbidden emission originating from the $^3\pi\pi^*$ levels. These effects, combined with the rigidification of the aromatic backbone by the complexation to $Gd(NO_3)_3$, eventually yield structured emission in time-resolved phosphorescence spectra, which reveals ligand-centred $^3\pi\pi^*$ levels located around 20 000 cm^{-1} (0–0 phonon) in these complexes (Table 5, Fig. S10c and S11c, ESI).†

In the Eu- and Tb-complexes, the ligand-centered luminescence is almost quantitatively quenched by efficient ligand → Ln^{III} energy transfer processes (Fig. S12, ESI).† Excitation through the $^1\pi\pi$ levels ($\tilde{\nu}_{exc}$ = 32 260 cm^{-1}) thus yields the standard red Eu-centered and green Tb-centered luminescence characterized by sharp bands

Table 5 Absorption (acetonitrile solution, 295K) and emission properties (solid state, 77K) of the ligands **L4**[b] and **L5** and of their complexes $[Ln(\mathbf{L4}^{b})(NO_3)_3]$ and $[Ln_2(\mathbf{L5})(NO_3)_6]$ (Ln = Eu, Gd, Tb)[a]

Compound	Absorption/ cm^{-1} $\pi \rightarrow \pi^*$	Emission/cm^{-1} $^1\pi\pi^*$	Emission/cm^{-1} $^3\pi\pi^*$	Lifetime/ ms τ ($^3\pi\pi^*$)	Lifetime/ ms τ (Ln*)	Quantum yield/%[b] ϕ_{Eu}^{L}
L4[b]	31 250	27 200 sh 26 315 21 740 sh	—	—	—	—
$[Gd(\mathbf{L4}^{b})(NO_3)_3]$	30 550	26 570 sh 23 810 br	20 600 19 250 17 920	1.91(1)	—	—
$[Eu(\mathbf{L4}^{b})(NO_3)_3]$	30 580	[c]	[c]	[c]	1.14(4) (77K)[d] 0.91(2) (295K)[d]	21(4)
$[Tb(\mathbf{L4}^{b})(NO_3)_3]$	30 550	[c]	[c]	[c]	1.11(4) (77K)[e] 0.38(3) (295K)[e]	—
L5	31 150	26 950 sh 25 500 24 200 sh	—	—	—	—
$[Gd_2(\mathbf{L5})(NO_3)_6]$	29 740	26 740 sh 25 510 23 640 sh	20 120 18 870 17 400	2.18(3)	—	—
$[Eu_2(\mathbf{L5})(NO_3)_6]$	29 590	[c]	[c]	[c]	0.95(2) (77K)[d] 0.68(4) (295K)[d]	21(4)
$[Tb_2(\mathbf{L5})(NO_3)_6]$	30 050	[c]	[c]	[c]	0.95(3) (77K)[e] 0.13(4) (295K)[e]	—

[a] sh = shoulder, br = broad. [b] Global quantum yield determined at 10^{-4} mol dm^{-3} in acetonitrile. [c] Ligand-centred luminescence quenched by transfer to Ln ion. [d] Lifetimes measured for $Eu(^5D_0)$ excited level. [e] Lifetimes measured for $Tb(^5D_4)$ excited level.

easily assigned to $Eu(^5D_0 \rightarrow {}^7F_j)$ (j = 0–6), $Eu(^5D_1 \rightarrow {}^7F_j)$ (j = 0–2), and $Tb(^5D_4 \rightarrow {}^7F_j)$ (j = 6–0) transitions (Fig. S12, ESI).†[53] The associated metal-centered lifetimes in the Eu-complexes at 77 K ($\tau_{Eu(5D0)}$ = 1.14(4) ms for $[Eu(\mathbf{L4b})(NO_3)_3]$ and $\tau_{Eu(5D0)}$ = 0.95(2) ms for $[Eu_2(\mathbf{L5})(NO_3)_6]$, Table 5), are typical for Eu^{III} coordinated by three bidentate nitrates, one tridentate aromatic binding unit and one solvent molecule.[50] They can be compared with $\tau_{Eu(5D0)}$ = 0.84 ms measured for $[Eu(\mathbf{L3}^{a})(NO_3)_3(CH_3OH)]$, and with $\tau_{Eu(5D0)}$ = 1.35 ms measured for $[Eu(\mathbf{L3}^{c})(NO_3)_3(CH_3CN)]$ in the same conditions (solid state, 77K).[50] The minor variation of $\tau_{Eu(5D0)}$ observed for $[Eu(\mathbf{L4b})(NO_3)_3]$ and $[Eu_2(\mathbf{L5})(NO_3)_6]$ in the 77–295 K range points to minor temperature effects on the non-radiative de-excitation processes affecting $Eu(^5D_0)$, in strong contrast with the 60–80% reduction in lifetime observed for the $Tb(^5D_4)$ level in the analogous Tb-complexes (Table 5). The latter standard behaviour is usually assigned to thermally-activated $Tb(^5D_4)$ → ligand($^3\pi\pi^*$) back transfer processes resulting from the minor energy gap separating these two levels in the complexes ($\Delta E_{gap} = E(^5D_4) - E(^3\pi\pi^*) \approx 20\,600$–$20\,000 = 600\ cm^{-1}$, Table 5).[18,53] Interestingly, the global quantum yields measured in acetonitrile are encouraging (ϕ_{Eu}^{L} = 21(4)% for both $[Eu(\mathbf{L4}^{b})(NO_3)_3]$ and $[Eu_2(\mathbf{L5})(NO_3)_6]$), and they compare well with ϕ_{Eu}^{L} = 25(4)% re-determined for $[Eu(\mathbf{L3}^{a})(NO_3)_3]$ in acetonitrile and using $Cs_3Eu(dipicolinate)_3$ complex as the unique reference in buffered water (see experimental section).[54]

Conclusion

The unsymmetrical tridentate N_2O binding unit in $\mathbf{L4}^{b}$ reacts with $Ln(NO_3)_3$ in acetonitrile to give ten-coordinated complexes $[Ln(\mathbf{L4}^{b})(NO_3)_3(CH_3CN)]$ very similar to those previously described with the analogous, but symmetrical N_3 binding unit in $[Ln(\mathbf{L3})(NO_3)_3(CH_3CN)]$.[18,34,50] The photophysical properties are also comparable, but $[Ln(\mathbf{L4}^{b})(NO_3)_3(CH_3CN)]$ do not show any sign of dimerization in solution, a process which drastically complicates the speciation of $[Ln(\mathbf{L3})(NO_3)_3(CH_3CN)]$ and affects its liquid crystalline properties when amphiphilic derivatives of the latter complexes are used as a building blocks in lanthanidomesogens.[18,34,55] The connection of two tridentate N_2O units *via* the diphenyl methane spacer in the ligand **L5** slightly reduces the absolute affinity of each binding site for $Ln(NO_3)_3$, but the planned saturated complexes $[Ln_2(\mathbf{L5})(NO_3)_6]$ complexes are quantitatively formed at millimolar concentrations in acetonitrile. The solid state structure of the binuclear complex $[Eu_2(\mathbf{L5})(NO_3)_6(H_2O)_2]$ confirms the fixation of ten-coordinated metals in the two adjacent tridentate binding sites, but a surprising helical twist of the spacer, comparable to that found in the triple-stranded complexes $[Ln_2(\mathbf{L5})_3]^{6+}$, results in a shorter intermetallic contact distance in the single-stranded complex (8.72 Å in $[Eu_2(\mathbf{L5})(NO_3)_6(H_2O)_2]$ and 9.06 Å in $[Tb_2(\mathbf{L5})_3](ClO_4)_6$). The combined analysis of experimental hydrodynamic radii and of NMR data indicates that the binuclear complexes $[Ln_2(\mathbf{L5})(NO_3)_6]$ adopt a flat and extended C_{2v}-symmetrical structure in acetonitrile, in which the Ln···Ln contact distance is increased by *c.a.* 30%. This unsymmetrical N_2O tridentate binding unit is thus ideally suited for producing simple and purely intermolecular complexation processes with $Ln(NO_3)_3$, which are amenable to reliable thermodynamic modeling. We observe that the successive connection of two neutral $Ln(NO_3)_3$ held at 12.3 Å in $[Ln_2(\mathbf{L5})(NO_3)_6]$ is anti-cooperative with a repulsive contribution of $\Delta E^{Ln,Ln} \approx 4\ kJ\ mol^{-1}$. The most surprising and striking conclusion of this contribution concerns the free energies of connection of the N_2O tridentate binding unit to $Ln(NO_3)_3$ ($\Delta G_{N2O}^{Ln,L}$) and the intermetallic interactions ($\Delta E^{Ln,Ln}$) in $[Ln_2(\mathbf{L5})(NO_3)_6]$, whose magnitudes closely match those found in the triple-stranded helicates $[Ln_2(\mathbf{L5})_3]^{6+}$ despite (i) the different nature of the entering metallic entity, a triply charged cation $[Ln(CH_3CN)_{8-9}]^{3+}$ for the latter complexes and a neutral $[Ln(NO_3)_3(CH_3CN)_3]$ unit

for the former complexes,[17] and (ii) the 30% increase of the intramolecular intermetallic contact distance in going from $[Ln_2(\mathbf{L5})_3]^{6+}$ to $[Ln_2(\mathbf{L5})(NO_3)_6]$ in solution. For the coordination chemists, this behaviour may be recognized as rather counter-intuitive since we are familiar with the interpretation of charge effects based on the exclusive use of point-charge Coulombic interactions, and we consider solvation effects mainly for their contribution to translational entropies.[56] However, these results support the current interpretation of intramolecular intermetallic interactions in polynuclear complexes as arising from two opposite contributions of comparable and huge magnitudes, one brought by intramolecular electrostatic interactions at the multi polar level[57] and the other associated with macroscopic solvation changes.[16,49]

Experimental

Solvents and starting materials

These were purchased from Fluka AG or Aldrich and used without further purification unless otherwise stated. The ligands **L4**^{b}[20] and **L5**[22] were prepared following previous strategies, but with improved specific procedures (Scheme S1, ESI†). Acetonitrile and dichloromethane were distilled over calcium hydride. Thin layer chromatography (TLC) used silica gel plates Merck 60 F_{254}, and Fluka silica gel 60 (0.04–0.063 mm) was used for preparative column chromatography. The nitrate salts $Ln(NO_3)_3{\cdot}xH_2O$ (Ln = La, Eu, Gd, Tb, Lu, Y; x = 2–4) were prepared from the corresponding oxides (Rhodia, 99.99%) and dried according to published procedures.[58] The Ln content of solid salts was determined by complexometric titrations with Titriplex III (Merck) in the presence of urotropine and xylene orange.[59]

Preparation of the complexes $[Ln(L4^{b})(NO_3)_3]{\cdot}xH_2O$ (Ln = La, x = 2.5; Ln = Eu, x = 2; Ln = Gd, x = 2.5; Ln = Tb, x = 2.5; Ln = Lu, x = 1.5; Ln = Y, x = 1.5) and $[Ln_2(L5)(NO_3)_6]{\cdot}xH_2O$ (Ln = La, x = 3; Ln = Eu, x = 3.5; Ln = Gd, x = 4; Ln = Tb, x = 3.5; Ln = Lu, x = 6; Ln = Y, x = 4)

A solution of $Ln(NO_3)_3{\cdot}xH_2O$ (Ln= La, Eu, Gd, Tb, Lu; Y, 0.06 mmol) in acetonitrile (5 cm^3) was added to a solution of either **L4**^{b} (19.3 mg, 0.06 mmol, 1 equiv.) or L5 (19.7 mg, 0.03 mmol, 0.5 equiv.) in acetonitrile (5 cm^3). After stirring for 1 h at rt, the solution was concentrated to 5 cm^3 and ^{t}butyl-methylether was slowly diffused for 24 h. The resulting microcrystalline powders were separated by filtration, dried (80 °C, 10^{-2} Torr) and yielded 75–85% of $[Ln(\mathbf{L4}^{b})(NO_3)_3]{\cdot}xH_2O$ (Ln = La, x = 2.5; Ln = Eu, x = 2; Ln = Gd, x = 2.5; Ln = Tb, x = 2.5; Ln = Lu, x = 1.5; Ln = Y, x = 1.5) and $[Ln_2(\mathbf{L5})(NO_3)_6]{\cdot}xH_2O$ (Ln = La, x = 3; Ln = Eu, x = 3.5; Ln = Gd, x = 4; Ln = Tb, x = 3.5; Ln = Lu, x = 6; Ln = Y, x = 4). All the complexes gave satisfying elemental analyses (Table S3, ESI).†

Spectroscopic and analytical measurements

Electronic spectra in the UV-vis were recorded at 293 K from solutions in MeCN with a Perkin-Elmer Lambda 900 spectrometer using quartz cells of 0.1 and 1 mm path length. Spectrophotometric titrations were performed with a J & M diode array spectrometer (Tidas series) connected to an external computer. In a typical experiment, 50 cm^3 of ligand in acetonitrile (10^{-4} mol dm^{-3}) were titrated at 293 K with a solution of $Ln(NO_3)_3{\cdot}xH_2O$ (10^{-3} mol dm^{-3}) in acetonitrile under an inert atmosphere. After each addition of 0.20 mL, the absorbance was recorded using Hellma optrodes (optical path length 0.1 cm) immersed in the thermostated titration vessel and connected to the spectrometer. Mathematical treatment of the spectrophotometric titrations was performed with factor analysis[46] and with the SPECFIT program.[47] IR spectra were obtained from KBr pellets with a FT-IR Perkin-Elmer Spectrum One. ^{1}H NMR spectra were recorded at 25 °C on Bruker Avance 400 MHz spectrometer. Chemical shifts are given in ppm with respect to TMS. Diffusion ordered spectroscopy (DOSY) was carried out at 400 MHz Larmor frequency (293 K, 10^{-2} mol dm^3, CD_3CN). The pulse sequence used was the Bruker pulse program ledbpgp2s[60] which employs stimulated echo, bipolar gradients and longitudinal eddy current delay as the z filter. The four 2 ms gradient pulses have sine-bell shapes and amplitudes ranging linearly from 2.5 to 50 G cm^{-1} in 32 steps. The diffusion delay was in the range 60–140 ms depending on the analyte diffusion coefficient, and the no. of scans was 32. The processing was done using a line broadening of 5 Hz and the diffusion coefficients were calculated with the Bruker processing package. Pneumatically-assisted electrospray (ESI-MS) mass spectra were recorded from 10^{-4} mol dm^{-3} solutions on a Finnigan SSQ7000 instrument. Elemental analyses were performed by Dr H. Eder from the microchemical Laboratory of the University of Geneva. Linear least-square fits were performed with Excel®. Emissison spectra, phosphorescence spectra and global quantum yields were determined using a Perkin Elmer LS50B fluorimeter. The quantum yields were calculated using the equation $\frac{\phi_x}{\phi_r} = \frac{A_r(\tilde{\nu}) \cdot I_r(\tilde{\nu}) \cdot n_x^2 \cdot D_x}{A_x(\tilde{\nu}) \cdot I_x(\tilde{\nu}) \cdot n_r^2 \cdot D_r}$, where x refers to the sample and r to the reference; A is the absorbance, $\tilde{\nu}$ the excitation wavenumber used, I the intensity of the excitation light at this energy, n the refractive index (n = 1.341 for acetonitrile solution and n = 1.330 for 0.1 mol dm^{-3} aqueous tris-buffer solution) and D the integrated emitted intensity. When $|A_r(\tilde{\nu}) - A_r(\tilde{\nu})| \geq 0.05$, the original exponential law was used $\frac{\phi_x}{\phi_r} = \frac{\left(1-10^{-A_r(\tilde{\nu})}\right) \cdot I_r(\tilde{\nu}) \cdot n_x^2 \cdot D_x}{\left(1-10^{-A_x(\tilde{\nu})}\right) \cdot I_x(\tilde{\nu}) \cdot n_r^2 \cdot D_r}$. Cs_3[Eu(2,6-pyridine-dicarboxylic acid)$_3$] (1.32×10^{-4} mol dm^{-3} in 0.1 mol dm^{-3} aqueous tris-buffer solution (pH = 7.45, from 1 mol dm^{-3} Sigma T2663, $\phi_r = 24\%$) was used as reference.[54] The excitation wavelength for the Eu-complexes was set to λ_{exc} = 279 nm. Elemental analyses were performed by Dr H. Eder from the Microchemical Laboratory of the University of Geneva.

Single-crystal structure determinations of $L4^{b}$, L5, $[Eu(L4^{b})(NO_3)_3(CH_3CN)](CH_3CN)_2$ (3) and $[Eu_2(L5)(NO_3)_6(H_2O)_2](H_2O)_4(CH_3CH_2CN)_2$ (4)

Summary of crystal data, intensity measurements and structure refinements are collected in Table S14 (ESI).† All crystals were mounted on quartz fibers with protection oil. Cell dimensions and intensities were measured at 150 K on a Stoe IPDS diffractometer with graphite-monochromated Mo-Kα radiation (λ = 0.71073 Å). Data were corrected for Lorentz and polarization effects and for absorption. The structures were solved by direct methods (SIR97),[61] all other calculation were performed with XTAL[62] system and ORTEP[63] programs.

Comments on the crystal structure of L4^b. The hydrogen atoms were observed and refined with isotropic displacement parameters, all other atoms were refined with anisotropic displacement parameters.

Comments on the crystal structure of L5. All non hydrogen atoms (49) were refined with anisotropic atomic displacement parameters. The hydrogen atoms were calculated and refined with $U_{iso} = 0.04$ Å^2, except for the terminal methyl groups, for which the atomic positions of the hydrogen atoms were refined with constraints on bond angles and on bond distances. The carbon atom of one terminal methyl group (C10) showed large atomic displacement parameters, but attempts to refine it on two different atomic positions did not improve convergence.

Comments on the crystal structure of [Eu(L4^b)(NO$_3$)$_3$-(CH$_3$CN)](CH$_3$CN)$_2$ (3). The atomic positions of the hydrogen atoms were calculated.

Comments on the crystal structure of [Eu$_2$(L5)(NO$_3$)$_6$-(H$_2$O)$_2$](H$_2$O)$_4$(CH$_3$CH$_2$CN)$_2$ (4). All non hydrogen atoms (45) were refined with anisotropic atomic displacement parameters. The hydrogen atoms were calculated and refined with $U_{iso} = 0.04$ Å^2, except for (i) the terminal methyl groups and (ii) the hydrogen atoms of the interstitial propionitrile solvent molecules for which the atomic positions of the hydrogen atoms were refined with constraints on bond angles and on bond distances. Among the three water molecules in the asymmetric unit, only O3w was slightly disordered and the propionitrile solvent molecule showed large displacement parameters. The complex was located onto a crystallographic twofold axis with C20 on special position (4*e*).

Acknowledgements

Financial support from the Swiss Office for Science and Education within the frame of the ESF COST Action D31 and from the Swiss National Science Foundation is gratefully acknowledged.

References

1 (*a*) R. E. P. Winpenny, *Chem. Soc. Rev.*, 1998, **27**, 447; (*b*) M. Sakamoto, K. Manseki and H. Okawa, *Coord. Chem. Rev.*, 2001, **219–221**, 379; (*c*) C. Benelli and D. Gatteschi, *Chem. Rev.*, 2002, **102**, 2369; (*d*) J.-C. G. Bünzli and C. Piguet, *Chem. Soc. Rev.*, 2005, **34**, 1048; (*e*) M. D. Ward, *Coord. Chem. Rev.*, 2007, **251**, 1663; (*f*) C. M. G. dos Santos, A. J. Harte, S. J. Quinn and T. Gunnlaugsson, *Coord. Chem. Rev.*, 2008, **252**, 2512.

2 (*a*) J.-C. G. Bünzli and C. Piguet, *Chem. Rev.*, 2002, **102**, 1897; (*b*) J. Hamacek, *J. Alloys and Compd.*, 2008, **451**, 347.

3 Y.-B. Dong, P. Wang, J.-P. Ma, X.-X. Zhao, H.-Y. Wang, B. Tang and R.-Q. Huang, *J. Am. Chem. Soc.*, 2007, **129**, 4872.

4 (*a*) T. Gross, F. Chevalier and J. S. Lindsey, *Inorg. Chem.*, 2001, **40**, 4762; (*b*) N. Ishikawa and Y. Kaizu, *Coord. Chem. Rev.*, 2002, **226**, 93; (*c*) K.-H. Schweikart, V. L. Malinovskii, A. A. Yasseri, J. Li, A. B. Lysenko, D. F. Bocian and J. S. Lindsey, *Inorg. Chem.*, 2003, **42**, 7431; (*d*) Y. Bian, L. Li, D. Wang, C.-F. Choi, D. Y. Y. Cheng, P. Zhu, R. Li, J. Dou, R. Wang, N. Pan, D. K. P. Ng, N. Kobayashi and J. Jiang, *Eur. J. Inorg. Chem.*, 2005, 2612; (*e*) J. Jiang and D. K. P. Ng, *Acc. Chem. Res.*, 2009, **42**, 79.

5 (*a*) S. J. A. Pope, A. M. Kenwright, S. L. Heath and S. Faulkner, *Chem. Commun.*, 2003, 1550; (*b*) S. Faulkner and S. J. A. Pope, *J. Am. Chem. Soc.*, 2003, **125**, 10526; (*c*) S. J. A. Pope, A. M. Kenwright, V. A. Boote and S. Faulkner, *Dalton Trans.*, 2003, 3780; (*d*) S. Faulkner and B. Burton-Pye, *Chem. Commun.*, 2005, 259; (*e*) M. S. Tremblay and D. Sames, *Chem. Commun.*, 2006, 4116.

6 (*a*) P. Guerriero, P. A. Vigato, J.-C. G. Bünzli and E. Moret, *J. Chem. Soc., Dalton Trans.*, 1990, 647; (*b*) K. D. Matthews, R. A. Fairman, A. Johnson, K. V. N. Spence, I. A. Kahwa, G. L. McPherson and H. Robotham, *J. Chem. Soc., Dalton Trans.*, 1993, 1719; (*c*) P. Froidevaux and J.-C. G. Bünzli, *J. Phys. Chem.*, 1994, **98**, 532; (*d*) J.-C. G. Bünzli and F. Ihringer, *Inorg. Chim. Acta*, 1996, **246**, 195; (*e*) R. C. Howell, K. V. N. Spence, I. A. Kahwa, A. J. P. White and D. J. Williams, *J. Chem. Soc., Dalton Trans.*, 1996, 961; (*f*) M. P. Oude Wolbers, F. C. J. M. van Veggel, R. H. M. Heeringa, J. W. Hofstraat, F. A. Geurts, G. J. van Hummel, S. Harkema and D. N. Reinhoudt, *Liebigs Ann.*, 1997, 2587; (*g*) R. C. Howell, K. V. N. Spence, I. A. Kahwa and D. J. Williams, *J. Chem. Soc. Dalton Trans.*, 1998, 2727; (*h*) L. J. Charbonnière, C. Balsiger, K. J. Schenk and J.-C. G. Bünzli, *J. Chem. Soc. Dalton Trans.*, 1998, 505; (*i*) M. K. Thompson, M. Vuchkov and I. A. Kahwa, *Inorg. Chem.*, 2001, **40**, 4332; (*j*) M. K. Thompson, A. J. Lough, A. J. P. White, D. J. Williams and I. A. Kahwa, *Inorg. Chem.*, 2003, **42**, 4828; (*k*) D. Sendor, M. Hilder, T. Juestel, P. C. Junk and U. H. Kynast, *New J. Chem,.*, 2003, **27**, 1070; (*l*) M. S. Tremblay, M. Halim and D. Sames, *J. Am. Chem. Soc.*, 2007, **129**, 7570; (*m*) L. Armelao, G. Bottaro, S. Quici, M. Cavazzini, M. C. Raffo, F. Barigelletti and G. Accorsi, *Chem. Commun.*, 2007, 2911; (*n*) D. T. de Lill, A. de Bettencourt-Dias and C. L. Cahil, *Inorg. Chem.*, 2007, **46**, 3960; (*o*) Y. Lv, J. Zhang, L. Wang, W. Cao and Z. Xu, *J. of. Luminesc.*, 2008, **128**, 117.

7 (*a*) J.-P. Costes, F. Dahan, A. Dupuis, S. Lagrave and J.-P. Laurent, *Inorg. Chem.*, 1998, **37**, 153; (*b*) J.-P. Costes and F. Nicodème, *Chem.–Eur. J.*, 2002, **8**, 3442; (*c*) J.-P. Costes, F. Dahan and F. Nicodème, *Inorg. Chem.*, 2003, **42**, 6556.

8 (*a*) N. André, R. Scopelliti, G. Hopfgartner, C. Piguet and J.-C. G. Bünzli, *Chem. Commun.*, 2002, 214; (*b*) N. André, T. B. Jensen, R. Scopelliti, D. Imbert, M. Elhabiri, G. Hopfgartner, C. Piguet and J.-C. G. Bünzli, *Inorg. Chem.*, 2004, **43**, 515; (*c*) T. B. Jensen, R. Scopelliti and J.-C. G. Bünzli, *Inorg. Chem.*, 2006, **45**, 7806; (*d*) T. B. Jensen, R. Scopelliti and J.-C. G. Bünzli, *Chem.–Eur. J.*, 2007, **13**, 8404; (*e*) T. B. Jensen, R. Scopelliti and J.-C. G. Bünzli, *Dalton Trans.*, 2008, 1027.

9 S. E. Plush and T. Gunnlaugsson, *Dalton Trans.*, 2008, 3801.

10 S. Tamburini, S. Sitran, V. Peruzzo and P. A. Vigato, *Eur. J. Inorg. Chem.*, 2009, 155.

11 (*a*) Y. Bretonnière, M. Mazzanti, J. Pécaut and M. M. Olmstead, *J. Am. Chem. Soc.*, 2002, **124**, 9012; (*b*) X.-Y. Chen, Y. Bretonnière, J. Pécaut, D. Imbert, J.-C. G. Bünzli and M. Mazzanti, *Inorg. Chem.*, 2007, **46**, 625.

12 (*a*) J. Hamacek, M. Borkovec and C. Piguet, *Chem.–Eur. J.*, 2005, **11**, 5217; (*b*) J. Hamacek, M. Borkovec and C. Piguet, *Chem. Eur. J.*, 2005, **11**, 5227; (*c*) J. Hamacek, M. Borkovec and C. Piguet, *Dalton Trans.*, 2006, 1473.

13 (*a*) D. Chapon, P. Delangle and C. Lebrun, *J. Chem. Soc., Dalton Trans.*, 2002, 68; (*b*) D. Chapon, J.-P. Morel, P. Delangle, C. Gateau and J. Pécaut, *Dalton Trans.*, 2003, 2745; (*c*) M. Borkovec, J. Hamacek and C. Piguet, *Dalton Trans.*, 2004, 4096.

14 N. Dalla Favera, J. Hamacek, M. Borkovec, D. Jeannerat, G. Ercolani and C. Piguet, *Inorg. Chem.*, 2007, **46**, 9312.

15 N. Dalla Favera, J. Hamacek, M. Borkovec, D. Jeannerat, F. Gumy, J.-C. G. Bünzli, G. Ercolani and C. Piguet, *Chem.–Eur. J.*, 2008, **14**, 2994.

16 G. Canard and C. Piguet, *Inorg. Chem.*, 2007, **46**, 3511.

17 J.-C. G. Bünzli and A. Milicic-Tang, in *Handbook on the Physics and Chemistry of Rare Earths*, ed. K. A. Gschneidner and L. Eyring, 1995, 21, 305.

18 (*a*) C. Piguet, A. F. Williams, G. Bernardinelli, E. Moret and J.-C. G. Bünzli, *Helv. Chim. Acta*, 1992, **75**, 1697; (*b*) E. Terazzi, S. Torelli, G. Bernardinelli, J.-P. Rivera, J.-M. Bénech, C. Bourgogne, B. Donnio, D. Guillon, D. Imbert, J.-C. G. Bünzli, A. Pinto, D. Jeannerat and C. Piguet, *J. Am. Chem. Soc.*, 2005, **127**, 888; (*c*) A. Escande, L. Guénée, K.-L. Buchwalder and C. Piguet, *Inorg. Chem.*, 2009, **48**, 1132.

19 M. Fréchette and C. Bensimon, *Inorg. Chem.*, 1995, **34**, 3520.

20 T. Le Borgne, P. Altmann, N. André, J.-C. G. Bünzli, G. Bernardinelli, P.-Y. Morgantini, J. Weber and C. Piguet, *Dalton Trans.*, 2004, 723.

21 S. Petoud, J.-C. G. Bünzli, F. Renaud, C. Piguet, K. J. Schenk and G. Hopfgartner, *Inorg. Chem.*, 1997, **36**, 5750.

22 (*a*) N. Martin, J.-C. G. Bünzli, V. McKee, C. Piguet and G. Hopfgartner, *Inorg. Chem.*, 1998, **37**, 577; (*b*) K. Zeckert, J. Hamacek, J.-P. Rivera, S. Floquet, A. Pinto, M. Borkovec and C. Piguet, *J. Am. Chem. Soc.*, 2004, **126**, 11589.

23 F. H. Allen, O. Kennard, D. G. Watson, L. Brammer, A. G. Orpen and R. Taylor, *J. Chem. Soc., Perkin Trans. 2*, 1987, S1.

24 H. Nozary, C. Piguet, J.-P. Rivera, P. Tissot, P.-Y. Morgantini, J. Weber, G. Bernardinelli, J.-C. G. Bünzli, R. Deschenaux, B. Donnio and D. Guillon, *Chem. Mater.*, 2002, **14**, 1075.
25 (*a*) E. C. Constable and D. G. F. Rees, *New J. Chem.*, 1997, **21**, 369; (*b*) M. J. Hannon, C. L. Painting, A. Jackson, J. Hamblin and W. Errington, *Chem. Commun.*, 1997, 1807; (*c*) C. He, C.-Y. Duan, C.-J. Fang and Q.-J. Meng, *J. Chem. Soc., Dalton Trans.*, 2000, 2419.
26 J. H. Brewster, *Top. Curr. Chem.*, 1974, **47**, 29.
27 (*a*) R. D. Shannon, *Acta Crystallogr.*, 1976, **A32**, 751; (*b*) J.-C. G. Bünzli, B. Klein, G. Chapuis and K. J. Schenk, *Inorg. Chem.*, 1982, **21**, 808.
28 (*a*) I. D. Brown and D. Altermatt, *Acta Crystallogr., Sect. B*, 1985, **41**, 244; (*b*) N. E. Brese and M. O'Keeffe, *Acta Crystallogr., Sect.. B*, 1991, **47**, 192; (*c*) I. D. Brown, *Acta Crystallogr., Sect. B*, 1992, **48**, 553; (*d*) I. D. Brown, *The Chemical Bond in Inorganic Chemistry*, Oxford University Press, UK, 2002.
29 (*a*) A. Trzesowska, R. Kruszynski and T. J. Bartczak, *Acta Crystallogr., Sect. B*, 2004, **60**, 174; (*b*) A. Trzesowska, R. Kruszynski and T. J. Bartczak, *Acta Crystallogr., Sect. B*, 2005, **61**, 429; (*c*) F. Zocchi, *THEOCHEM*, 2007, **805**, 73.
30 J.-C. G. Bünzli, *Handbook on the Physics and Chemistry of Rare Earths*, ed. K. A. Gschneider, Jr and L. Eyring, Elsevier, 1987, ch. 60, 322.
31 D. K. Lavallee, M. D. Baughman and M. P. Phillips, *J. Am. Chem. Soc.*, 1977, **99**, 718.
32 (*a*) G. R. Choppin, *Lanthanide Probes in Life, Chemical and Earth Sciences*, ed. J.-C. G. Bünzli and G. R. Choppin, Elsevier, 1989; (*b*) N. Kaltsoyannis and P. Scott, *The f Elements*, Oxford Science Publication, Oxford, 1999.
33 M. Pons and O. Millet, *Prog. Nucl. Magn. Reson. Spectrosc.*, 2001, **38**, 267.
34 (*a*) H. Nozary, C. Piguet, P. Tissot, G. Bernardinelli, J.-C. G. Bünzli, R. Deschenaux and D. Guillon, *J. Am. Chem. Soc.*, 1998, **120**, 12274; (*b*) H. Nozary, C. Piguet, J.-P. Rivera, P. Tissot, G. Bernardinelli, N. Vulliermet, J. Weber and J.-C. G. Bünzli, *Inorg. Chem.*, 2000, **39**, 5286.
35 (*a*) P. Stilbs, *Progr. NMR Spectrosc.*, 1986, **19**, 1; (*b*) A. R. Waldeck, P. W. Kuchel, A. J. Lennon and B. E. Chapman, *Progr. NMR Spectrosc.*, 1997, **30**, 39; (*c*) P. S. Pregosin, E. Martinez-Viviente and P. G. Anil Kumar, *Dalton Trans.*, 2003, 4007; (*d*) A. Macchioni, G. Ciancaleoni, C. Zuccaccia and D. Zuccaccia, *Chem. Soc. Rev.*, 2008, **37**, 479.
36 A. Gierer and K. Z. Wirtz, *Z. Naturforsch., A*, 1953, **8**, 532.
37 H.-C. Chen and S.-H. Chen, *J. Phys. Chem.*, 1984, **88**, 5118.
38 L. Allouche, A. Marquis and J.-M. Lehn, *Chem.–Eur. J.*, 2006, **12**, 7520.
39 (*a*) M. L. Connolly, *Science*, 1983, **221**, 709; (*b*) M. L. Connolly, *J. Appl. Crystallogr.*, 1983, **16**, 548.
40 S. J. Candau, in *Surfactant Solutions*, ed. R. Zana, Marcel Dekker Inc., New York and Basel, 1987, pp. 157–158.
41 (*a*) J. Perrin, *J. Phys. Radium*, 1934, **5**, 497; (*b*) J. Perrin, *J. Phys. Radium*, 1936, **7**, 1.
42 M. M. Tirado, C. L. Martinez and J. Garcia De La Torre, *J. Chem. Phys.*, 1984, **81**, 2047.
43 J. Garcia De La Torre and V. A. Bloomfield, *Biopolymers*, 1977, **16**, 1747.
44 B. Hamelin, L. Jullien, C. Derouet, C. Hervé du Penhoat and P. Berthault, *J. Am. Chem. Soc.*, 1998, **120**, 8438.
45 (*a*) 1 C. Piguet, J.-C. G. Bünzli, G. Bernardinelli, C. G. Bochet and P. Froidevaux, *J. Chem. Soc., Dalton Trans.*, 1995, 83; (*b*) E. Terazzi, L. Guénée, P.-Y. Morgantini, G. Bernardinelli, B. Donnio, D. Guillon and C. Piguet, *Chem.–Eur. J.*, 2007, **13**, 1674.
46 E. R. Malinowski and D. G. Howery, *Factor Analysis in Chemistry*, Wiley, New York, Chichester, 1980.
47 (*a*) H. Gampp, M. Maeder, C. J. Meyer and A. D. Zuberbühler, *Talanta*, 1986, **33**, 943; (*b*) H. Gampp, M. Maeder, C. J. Meyer and A. D. Zuberbühler, *Talanta*, 1985, **23**, 1133.
48 G. Ercolani, C. Piguet, M. Borkovec and J. Hamacek, *J. Phys. Chem. B*, 2007, **111**, 12195.
49 (*a*) L. Onsager, *J. Am. Chem. Soc.*, 1936, **58**, 1486; (*b*) D. V. Matyushov, *J. Chem. Phys.*, 2004, **120**, 1375.
50 S. Petoud, J.-C. G. Bünzli, K. J. Schenk and C. Piguet, *Inorg. Chem.*, 1997, **36**, 1345.
51 W. T. Carnall, P. R. Fields and K. Rajnak, *J. Chem. Phys.*, 1968, **49**, 4443.
52 (*a*) S. Tobita, M. Arakawa and I. Tanaka, *J. Phys. Chem.*, 1984, **88**, 2697; (*b*) S. Tobita, M. Arakawa and I. Tanaka, *J. Phys. Chem.*, 1985, **89**, 5649.
53 J.-C. G. Bünzli and C. Piguet, *Chem. Soc. Rev.*, 2005, **34**, 1048.
54 A.-S. Chauvin, F. Gumy, D. Imbert and J.-C. G. Bünzli, *Spectrosc. Lett.*, 2004, **37**, 517; Erratum: *Spectroscopy Lett.*, 2006, **40**, 193.
55 (*a*) E. Terazzi, B. Bocquet, S. Campidelli, B. Donnio, D. Guillon, R. Deschenaux and C. Piguet, *Chem. Commun.*, 2006, 2922; (*b*) T. B. Jensen, E. Terazzi, B. Donnio, D. Guillon and C. Piguet, *Chem. Commun.*, 2008, 181.
56 R. J. Motekaitis, A. E. Martell and R. A. Hancock, *Coord. Chem. Rev.*, 1994, **133**, 39, and references therein.
57 (*a*) A. L. Thompson, D. Parker, D. A. Fulton, J. A. K. Howard, S. U. Pandya, H. Puschmann, K. Senanayake, P. A. Stenson, A. Badari, M. Botta, S. Avedano and S. Aime, *Dalton Trans.*, 2006, 5605; (*b*) C. J. Cramer and D. G. Truhlar, *Acc. Chem. Res.*, 2008, **41**, 760.
58 J. F. Desreux, in *Lanthanide Probes in Life, Chemical and Earth Sciences* ed. J.-C. G. Bünzli and G. R. Choppin, Elsevier, Amsterdam, 1989, ch. 2, p. 43.
59 G. Schwarzenbach, *Complexometric Titrations*, Chapman & Hall, London, 1957, p. 8.
60 D. Wu, A. Chen and C. S. Johnson, Jr, *J. Magn. Reson., A*, 1995, **115**, 260.
61 A. Altomare, M. C. Burla, M. Camalli, G. Cascarano, C. Giacovazzo, A. Guagliardi, G. Moliterni, G. Polidori and R. Spagna, *J. Appl. Crystallogr.*, 1999, **32**, 115.
62 *XTAL 3.2 User's Manual*, ed. S. R. Hall, H. D. Flack and J. M. Stewart, Universities of Western Australia and Maryland, 1989.
63 C. K. Johnson, *ORTEP II; Report ORNL-5138*, Oak Ridge National Laboratory, Oak Ridge, Tennessee, 1976.

